Assessment of separation efficiency modeling and visualization approaches pertaining to flow and mixing patterns on distillation trays

Vishwakarma, V.; Schubert, M.; Hampel, U.;

Originally published:

March 2018

Chemical Engineering Science 185(2018), 182-208

DOI: https://doi.org/10.1016/j.ces.2018.03.052

Perma-Link to Publication Repository of HZDR:

https://www.hzdr.de/publications/Publ-25436

Review Article

ASSESSMENT OF SEPARATION EFFICIENCY MODELING AND VISUALIZATION APPROACHES PERTAINING TO FLOW AND MIXING PATTERNS ON DISTILLATION TRAYS

Vineet Vishwakarma[a,b], Markus Schubert[a,*], Uwe Hampel[a,b]

[a]Helmholtz-Zentrum Dresden-Rossendorf, Institute of Fluid Dynamics, Bautzner Landstraße 400, 01328 Dresden, Germany

[b]Technische Universität Dresden, AREVA Endowed Chair of Imaging Techniques in Energy and Process Engineering, 01062 Dresden, Germany

*Corresponding author: Tel.: +49 351 260 2627, Fax: +49 351 260 2383

E-mail address: m.schubert@hzdr.de

Abstract: Distillation columns are essential to chemical process industries, and most of them are fitted with cross-flow trays due to their versatility. Since these columns are expensive in terms of cost and energy consumption, an accurate determination of their separation efficiency is a prerequisite to optimization of their performance by design modification and revamping. This would further reduce the extra trays, added to account for the uncertainties, during the column design leading to energy efficient operation. There have been several attempts in the past to understand the nature of liquid mixing and flow patterns on the trays through experiments and CFD simulations, and to relate them with their separation efficiency through CFD, empirical and theoretical models. The present work aims at reviewing the experimental and the simulation studies accomplished to characterize the flow and the mixing patterns on column trays. In particular, a comprehensive review of the existing theoretical efficiency prediction models along with the critical analysis of their strengths and weaknesses is presented. The dependence of the

tray efficiency on system and flow properties is also discussed. In addition, a concise strategy on how to process and utilize the experimental data in tandem with mathematical models is proposed. The future of the tray efficiency modeling is anticipated to feature hybrid approaches, i.e. using theoretical models supplemented with fluid dynamics information from experimentally validated CFD models. Thus, the knowledge of the existing theoretical approaches is imperative for their improvement and development of the new ones for better tray efficiency predictions.

Keywords: Distillation tray, tray efficiency, flow and mixing patterns, CFD, experiments, flow maldistribution.

1. Background

Distillation is the most important separation technology and will be pursued in the future simply due to the unavailability of industrially viable alternatives.[1] The physical separation of component substances from their mixture, called feed, is achieved in distillation columns.[2] Distillation columns are widely regarded as the workhorses of petroleum, chemical, petrochemical and related process industries.[3] These units consume approximately 3% of the total energy of the world,[4] and about 50% of the total process energy in chemical and petroleum refineries.[2] They also incur up to 50% of capital and operating costs in industrial processes.[2] These statistics certify distillation processes as the biggest energy consumers and the largest single investments in chemical industries. Increasing energy costs and higher awareness for environmental concerns motivate the scientific community to reconsider these cost- and energy-intensive process equipments for improved designs as well as higher efficiencies.

Distillation columns are equipped with internals - primarily trays or packings or combination of both.[2] The internals enhance the contact and the mass transfer between liquid and vapor phase inside the column, which is essential for an efficient component separation. The selection of the

type of internals depends on several factors such as liquid and vapor load, operating pressure and pressure drop, cost, sensitivity to fouling and corrosion, inspection access, revamping, experience and so forth.[2] Around half of the columns in the world are tray columns and the other half are random and structured packing columns together.[2] The present work is concerned towards the modeling approaches related with the columns fitted with cross-flow trays, which is the most common tray configuration.[2] Further, as the column is a cascade of trays with more or less same geometry and function, the modeling of the columns could be reduced to the consideration of mass and enthalpy flow on one tray only.

The term 'efficiency' is preferred to account for the separation duty of a tray. However, several definitions of efficiency, with reference to tray columns exist in the literature.[5] The simplest interpretation is the overall column efficiency (E_o), which is defined as

$$E_o = \frac{N_{eq}}{N_{ac}} \quad . \tag{1}$$

This is also known as the overall stage efficiency. Here, N_{eq} is the number of equilibrium stages, obtained from equilibrium design calculations (McCabe-Thiele method), the Fenske-Underwood-Gilliland method, process engineering softwares or from others,[2] while N_{ac} is the actual number of trays in a column. The achievement of separation on a cross-flow tray is usually described by the (Murphree[6]) tray efficiency. It is the ratio of the actual change in vapor[1] composition on a tray over its composition change for an equivalent equilibrium stage, according to

$$E_{MV} = \frac{y_m - y_{in}}{y_m^* - y_{in}} \quad . \tag{2}$$

E_{MV} is the vapor-side tray efficiency as the composition change of vapor is considered. Here, y_m is the composition of the vapor leaving the m^{th} tray whereas y_m^* is its composition in equilibrium with the liquid exiting the same tray (refer Fig. 1). The vapor composition y_{in} is homogenous due to the assumption of perfectly mixed incoming vapor. This supposition has been practiced in

[1] The term 'gas' and 'vapor' are used interchangeably in this work.

numerous research articles and is only applicable to small diameter columns.[7] Large columns often do not have sufficient distance between the consecutive trays for the vapor to get completely mixed.[7] Moreover, the Murphree tray efficiency is pertinent for completely mixed liquid, i.e. without any liquid concentration gradient on the tray, which does not happen in reality. For large columns and systems with high relative volatilities, the liquid composition x_m is sometimes lower than its composition in equilibrium with the outgoing vapor i.e. y_m. Due to this reason, y_m^* becomes less than y_m, causing the tray efficiency to exceed unity.[3,8]

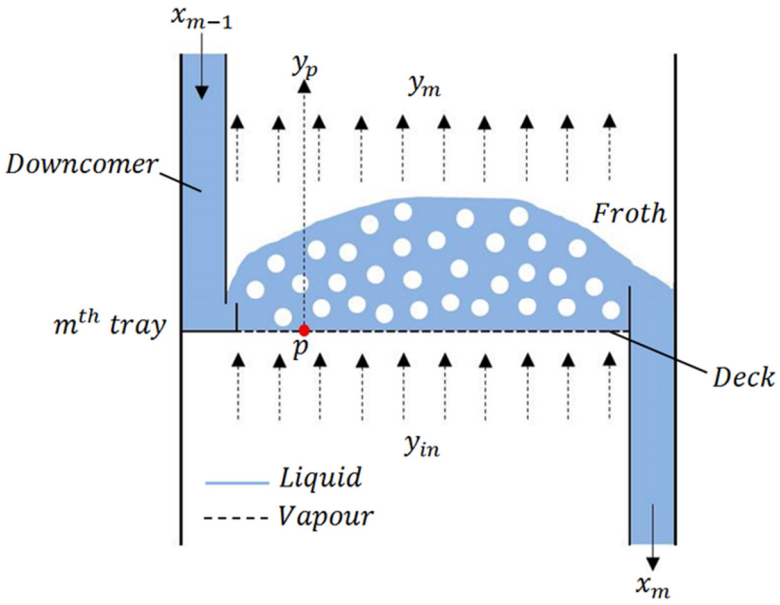

Fig. 1. Illustration for vapor-side tray and point efficiency.

Similar to the tray efficiency, the Murphree point efficiency is the actual composition change per equilibrium change at a particular point on the tray. The vapor-side point efficiency at point *p* on the tray is defined as

$$E_{OG} = \frac{y_p - y_{in}}{y_p^* - y_{in}} \quad . \tag{3}$$

y_p and y_p^* are the vapor compositions that are actual and in equilibrium with the liquid at that point, respectively, as shown in Fig. 1. This definition of the vapor-side point efficiency is more realistic than the tray efficiency as it considers the composition variation along the tray.[2] The difference between the vapor-side tray efficiency and the point efficiency arises due to the varia-

tion in the equilibrium vapor composition across the tray according to the liquid composition profile.[9] Analogous expressions for liquid-side tray and point efficiency can be formulated.[2,3] The tray efficiency is same as the point efficiency, when both liquid and vapor phases are completely mixed. However, the Murphree tray efficiency is usually higher than the point efficiency due to the cross-flow of gas and liquid.[10] Other definitions of the tray efficiency were proposed for example by Hausen,[11] Standart,[12] and Holland[13,14]. Recently, Jaćimović and Genić[15,16] proposed the normalized tray efficiency (i.e. the ratio of the real tray mass transfer rate to the theoretical maximum mass transfer rate), which is same for both phases and lies within zero and unity. The acknowledgement of any other efficiency concept than Murphree's by the process industry is yet to be noticed. Since the phases are partially mixed, a phenomenological model incorporating the mixing patterns of liquid and vapor is required for converting the point efficiency to the tray efficiency.[3] Further, the efficiencies in Eqs. 3 and 4 are valid for binary mixtures. For multicomponent mixtures, the pseudo-binary approach is preferred to retain the simple method with only minor changes.[5]

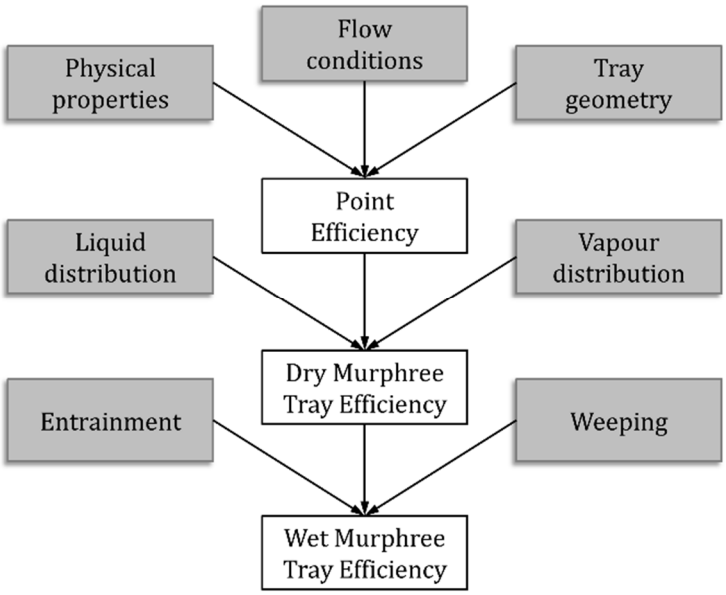

Fig. 2. Classification of the tray efficiency.

Further classification of the tray efficiency and the factors affecting it can be understood from Fig. 2.[17] The point efficiency refers to the mass transfer at a certain point on the tray depending

on local flow conditions, physical properties of the fluids and geometry of the system. Similarly, the tray efficiency is a function of (i) geometrical design parameters of the tray, (ii) physical properties of the system (e.g. density, viscosity, surface tension, etc.) and (iii) overall operating conditions such as vapor and liquid loads. This efficiency is also known as 'Dry Murphree Tray Efficiency'. When the additional effects of entrainment and weeping (which are unfavorable for the tray or column performance) are further assimilated, the tray efficiency transforms to 'Wet Murphree efficiency'.[17]

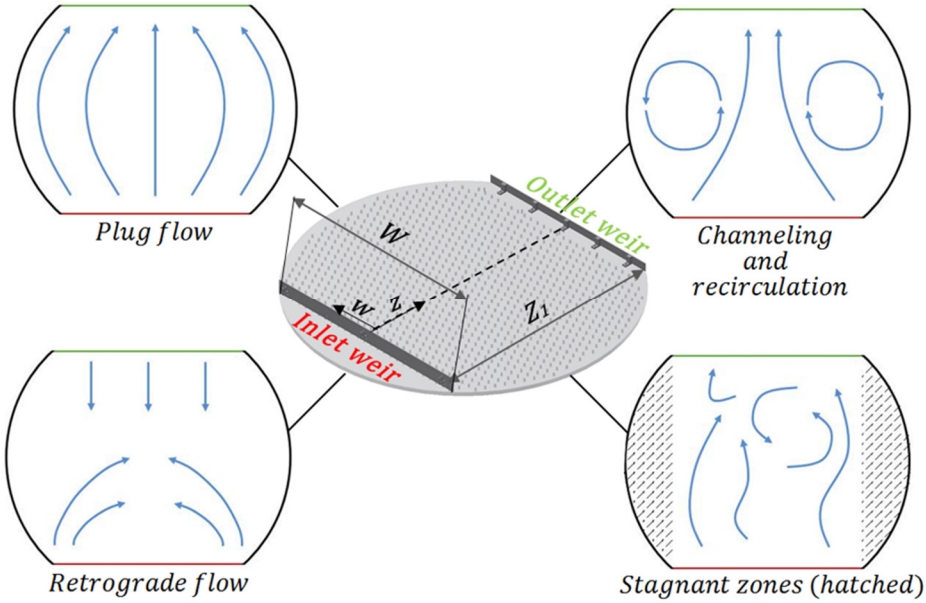

Fig. 3. Liquid flow patterns on a tray.

The fashion in which the fluidic phases flow over the tray has strong influence on its mass transfer performance. Several studies concerning the experimental identification of the liquid flow at different design and operating conditions prompted the development of mathematical models to account for liquid maldistribution only. In general, the term 'flow non-idealities' is used to refer to liquid maldistribution. On the contrary, no attempts to quantify the vapor non-idealities through experiments have been made due to which the vapor flow is assumed in these models as stated earlier. Besides, the plug flow of liquid is known to be beneficial for the efficiency and is termed 'ideal' for the trays. On the other hand, non-ideal flow patterns, such as liquid channeling,

bypassing, retrograde flow and the presence of re-circulation and stagnant zones,[18] as shown in Fig. 3,[19] are detrimental to the tray efficiency.[20]

2. Experimental and Numerical Flow Visualization

Since the knowledge of the prevailing flow patterns is important for the evaluation of the tray efficiency, different experimental and numerical techniques have been devised to visualize the flow fields on the trays. These techniques are discussed successively hereafter.

2.1 Experimental Studies

The simplest experimental method involved the usage of floats, such as table-tennis or cork balls, to pursue the flow of liquid.[21,22] However, slip velocities between the liquid surface and the balls as well as velocity gradients along the froth height limit the accuracy of this method. The flow of liquid using colored dye and photographic camera was once visualized by Porter et al.[21] In other studies, flow patterns were obtained from isotherms in the liquid, while the tray was operated with hot water and cold air, and local liquid temperatures were measured with thermocouples[10] and thermometers[23] at multiple locations. Multiple flow pointers, like weather vanes, were also used to detect the flow direction on a tray, despite of being highly intrusive to the flow itself.[23] Yet, infrared camera technique was used to visualize the fronts of inflowing hot liquid mixing with cold liquid.[24] The extraction of quantitative flow parameters with these techniques was still difficult. The strain gauge probe technique was employed by Biddulph and Bultitude[25] to obtain unidirectional velocity fields. However, the calibration of such probes is challenging, as they need to be adjusted for every froth condition. Solari and Bell[26] and Bell[27,28] extensively utilized fiber optic techniques and fluorescent tracer to acquire flow and mixing patterns using residence time profiles. Until now, the results from these experiments are preferably used as validating criteria for numerical models (Computation Fluid Dynamics - CFD) discussed

147 later. Yu et al.[29] employed conductivity probes to trace the liquid flow using salt solution as trac-
148 er; however, the spatial resolution of recorded data is rather low. The nature of liquid flow at
149 different elevations above the tray deck was identified by Liu et al.[30] using a hot film anemome-
150 ter. Recently, Schubert et al.[18] used a wire-mesh sensor to measure the residence time distribu-
151 tion and velocity fields distributed on a tray at uniquely high spatial and temporal resolution. A
152 consolidated list of existing experimental techniques to identify the flow behavior on column
153 trays is given in Tab. 1.

154 **Space left for Table 1**

155 **Tab. 1.** Summary of literature on experimental methods concerning column tray flow patterns.

Reference	Tray setup; gas/ liquid system	Technique	Observations
Stichlmair and Ulbrich[10]	Ø = 2.30 m bubble-cap and sieve tray; hot water/ air	Thermocouples	Liquid isotherms indicate the extent of channeling; influence of modified inlet and outlet weirs, tray tilting and baffles on flow patterns.
Biddulph and Bultitude[25]	Ø = 0.69 m sieve tray; water/ air	Strain gauge probe network	Axial velocity profiles show non-uniform flow of liquid with low velocities near the wall.
Sohlo and Kinnunen[22]	Ø = 0.50 m sieve tray; water/ air	Floating cork balls	Non-ideal velocity profiles at low liquid flow rates and at high weir heights; plug flow behavior at high liquid flow rates and at low weir heights.
Porter et al.[23]	Ø = 2.44 m sieve tray; hot water/ air	Thermometers, flow pointers	Substantial liquid recirculation at high weir loads and at low gas loads.
Porter et al.[21]	Ø = 1.20 m sieve tray; water/ air	Photographic camera, dye injection, table-tennis balls	Existence of stagnant regions near the wall; tray tilting modifies the liquid flow patterns.
Solari and Bell[26]	Ø = 1.20 m sieve tray; water/ air	Fiber-optic detection system, dye injection	Liquid pooling near the wall at low liquid and gas loads; effect of flow rates on this pooling; existence of non-ideal flow and mixing patterns.
Li et al.[24]	Ø = 1.20 m sieve tray; water/ air	Thermal infrared camera, hot water injection	Flow non-uniformity on the tray with one downcomer; stagnant regions on multiple downcomer tray depicted through frontier curves.
Yu et al.[29]	Ø = 2.00 m sieve tray; water/ air	Electrical conductivity probes, tracer injection	Non-uniform (parabolic) flow in the central part of the tray with slow re-circulation near the wall.
Liu et al.[30]	Ø = 1.20 m sieve tray; water/ air	Hot film anemometer	3D flow of liquid up to 10 mm above the tray deck and the flow becomes 2D beyond the aforementioned distance.
Schubert et al.[18]	Ø = 0.80 m sieve tray; water/ air	Wire mesh sensor, tracer injection	Influence of liquid load and outlet weir on flow patterns; liquid RTD and weir-to-weir velocities portraying flow non-idealities.

2.2 CFD Simulations

In addition to the advances in experimental techniques, CFD has progressively emerged as an important tool[30-42] for understanding the complex two-phase flows on distillation trays and to forecast the tray performance at best prior to construction for various designs and operating conditions.[34] In the past 25 years, several attempts have been made to model the tray hydrodynamics. All CFD studies discussed here use the Eulerian framework, if not otherwise specified. Mehta et al.[31] predicted the steady-state three-dimensional flow of the liquid on a sieve tray, using time- and volume-averaged continuity and momentum equations for the liquid phase only. Interactions with the vapor phase were considered using interphase momentum transfer coefficients determined from empirical correlations. Krishna et al.[32] and Van Baten and Krishna[33] advanced the previous approach by proposing a three-dimensional two-phase model to simulate the sieve tray hydrodynamics. They modeled the turbulent gas-liquid flow by assuming the momentum exchange through bubble-liquid interactions only. It should be further mentioned that their work was focused on small trays, where fluid dynamics is inconsistent with that of industrial trays. Also, they estimated the interphase momentum exchange coefficient based on the correlation of Bennett et al.[43], which overpredicts the liquid holdup fraction in the froth regime. Liu et al.[30] studied the two-phase flow behavior on a sieve tray with a relatively simple two-dimensional model. They ignored the variations along the dispersion height in the direction of gas flow, modeled the gas action with an empirical equation and described the hydrodynamics of the liquid phase only. Gesit et al.[34] employed a three-dimensional model and used the liquid holdup correlation suggested by Colwell[44] to predict the flow patterns and hydraulics of a commercial-scale sieve tray. According to Kister[3], different correlations can lead to inconsistent and widely-varying predictions of the tray hydrodynamics.[45] Further, two-dimensional simulations cannot account for the existing flow variations in the vertical dimension. Previously described attempts were only concerned towards tray hydrodynamics, while they neglected mass and energy conservation on sieve trays. As a result, Wang et al.[35] established a three-dimensional pseudo-single-fluid model for obtaining liquid phase velocity and concentration distributions on

sieve trays in a 10-trayed column. A single-fluid model was preferred over a more accurate two-phase model for simulating an entire column due to its simplicity and low computational cost. They performed the mass transfer studies for cyclohexane – n-heptane system and estimated the overall column efficiency using the Fenske-Underwood equation[35], which was overpredicted with reference to Sakata and Yanagi[46]. This method of determining the column efficiency using end-product specifications is apt for approximate estimations only.[47] Error accumulation due to simultaneous solution of momentum and mass-transfer equation and the usage of eddy-diffusion coefficient from the correlations applicable for air-water system only are the other reasons behind this overprediction. The assumption of constant values for vapor (and liquid) volume fractions and the inability to predict point and tray efficiencies are further limitations of this model. Rahimi et al.[36] and Noriler et al.[37,38] extended the two-phase CFD model by considering the energy and the chemical species conservation in a three-dimensional framework. They used correlations for momentum, heat and mass-transfer coefficients to predict hydrodynamics along with temperature and concentration distributions on rectangular and circular sieve trays. However, the employment of standard correlations and empirical models for simulating the heat and mass-transfer on sieve trays is questionable.[47] Zarei et al.[48] compared the hydrodynamic performance of a mini V-grid (MVG) valve tray and a sieve tray with a two-phase three-dimensional model. The simulations indeed exhibited higher capacity for the MVG tray than for the geometrically similar sieve tray, however, no experimental validation of the hydrodynamics of MVG valve tray was attempted in their work. The effect of the holes and bubble diameters on hydraulics and mass transfer performance of two geometrically similar sieve trays was investigated by Rahimi et al.[49] using a three-dimensional two-phase model. They used a steady state model, which is insufficient for modeling the dynamical behavior of distillation trays. Recently, several investigators focused on the application of CFD studies to non-conventional trays. Jiang et al.[50] and Li et al.[39] examined the tray hydraulics on a fixed valve tray through a two-phase three-dimensional transient CFD model. Their models underpredicted the clear liquid height with respect to experimental data. Jiang et al.[51] developed a two-phase three-dimensional model

to study the hydrodynamics and mass-transfer behavior of a ripple tray, i.e. a special form of a dual tray. A mismatch between CFD prediction and experiments concerning the froth height led to a disagreement in the tray efficiency. Sun et al.[52] used a three-dimensional two-phase model with a realizable k-ε turbulence model to simulate the tray hydrodynamics on a cross-orthogonal fixed valve tray. Similar analysis was also done by Li et al.[41] for a sieve tray with flow-guided holes and a bubble-promoter. The scope of their investigations were limited to hydrodynamics, while their predictions were inconsistent with the correlations and experimental data.[41,52] Another study regarding the tray hydrodynamics in a sieve tray column under different inclinations due to wind loads was conducted by Ping et al.[40] using the volume of fluid (VOF) method. The interface curvature and surface tension forces are difficult to model correctly with this model, thereby affecting the interface shape.[53] The prediction of clear liquid height through this method was inconsistent with the Francis' equation and the experiment.[40] A hybrid approach of the volume of fluid (VOF) and a large eddy simulation (LES) model was developed by Malvin et al.[54] to reduce the computational cost of the simulations. Although velocity predictions were in good agreement with Solari and Bell[26] experiments, the same is not true for the clear liquid height with respect to Solari and Bell[26], Colwell[44] and Bennett et al.[43]. Li et al.[55] proposed the concept of an 's' shaped distillation column fitted with elliptical sieve trays. They established the importance of this unconventional tray by comparing its hydraulics, RTD and mass-transfer performance with a conventional sieve tray, using two-phase three-dimensional model. Since no such column exists in reality, this study lacked the experimental validation of the predictions. Another unconventional tray known as conical cap (ConCap) tray was examined by Zarei et al.[42], using a VOF-like code with multiple size group (MUSIG) and shear stress transport (SST) model. The total pressure drop of the ConCap tray was underpredicted by their model with respect to their experiments[56]. A consolidated summary of the reported CFD analyses of distillation trays is given in Tab. 2.

235 **Tab. 2.** Summary of literature on CFD studies for predicting the tray performance.

Reference	Multiphase model	Tray setup; gas / liquid system	Observations
Mehta et al.[31]	3D, steady state, single phase, continuum based model	Ø = 1.21 m sieve tray; water/ air	Liquid velocity distribution
Krishna et al.[32]	3D, transient, two phase, Euler-Euler	0.39 m x 0.22 m sieve tray; water/ air	Liquid velocity vectors and streamlines, volume fraction distribution, liquid holdup distribution and clear liquid height
Van Baten and Krishna[33]		Ø = 0.30 m sieve tray; water/ air	
Liu et al.[30]	2D, steady state, single phase, k-ε turbulence model	Ø = 1.20 m sieve tray; water/ air	Liquid velocity vectors and circulation area
Gesit et al.[34]	3D, transient, two phase, Euler-Euler	Ø = 1.22 m sieve tray; water/ air	Velocity distribution and streamlines of liquid and gas, liquid velocity vectors, clear liquid height, froth height, liquid holdup and volume fraction profiles
Wang et al.[35]	3D, steady state, pseudo-single-phase, k-ε turbulence model	Ø = 1.22 m sieve trays (10 nos.) in a column; water/ air, and cyclohexane/ n-heptane	Liquid velocity distribution and vector plots, liquid concentration profiles and overall column efficiency
Rahimi et al.[36]	3D, transient, two phase, Euler-Euler	1.07 m x 0.09 m sieve tray; methanol/ n-propanol, and ethanol/ n-propanol. Ø = 1.2 m sieve tray; cyclohexane/ n-heptane	Liquid composition and temperature profiles, point and tray efficiency
Noriler et al.[37,38]	3D, transient, two phase, Euler-Euler	Ø = 0.35 m sieve tray; water/ air, and ethanol/ water	Liquid holdup, clear liquid height, pressure drop, gas and liquid velocity profiles and streamlines, liquid velocity and temperature distributions, mass and volume fraction, and point and tray efficiency
Zarei et al.[48]	3D, steady state, two phase, Euler-Euler	Ø = 1.21 m mini V-grid (MVG) valve and sieve tray; water/ air	Liquid velocity distribution, liquid and gas velocity vectors, clear liquid height, froth height, liquid holdup, pressure drop and liquid volume fraction profiles and streamlines
Jiang et al.[50]	3D, transient, two phase, Euler–Euler	Ø = 0.60 m fixed triangular valve tray; water/ air	Clear liquid height, holdup distribution and velocity vectors of gas and liquid, liquid velocity distribution and streamlines
Rahimi et al.[49]	3D, steady state, two phase, Euler–Euler	Two rectangular (0.99 m x 0.08m) sieve trays with different hole dia.; methanol/ n-propanol	Clear liquid height, froth height, liquid velocity profile, liquid and vapor phase mole fraction, liquid volume fraction contours, point and tray efficiency

Jiang et al.[51]	3D, steady state, two phase, Euler–Euler	Ø = 0.31 m ripple trays with different free area; cyclohexane/ n-heptane	Clear liquid height, froth height, liquid velocity distribution and volume fraction, vapor phase mole fraction, interfacial area density and tray efficiency
Li et al.[39]	3D, transient, two phase, Euler–Euler	Ø = 0.60 m fixed valve tray; water/ air	Holdup distribution, velocity vectors and streamlines of liquid and gas, gas-liquid interface profile, clear liquid height and gas velocity distribution
Sun et al.[52]	3D, transient, two phase, Euler-Euler, realizable k-ε model	Ø = 1.20 m cross-orthogonal fixed-valve tray; water/ air	Clear liquid height, gas holdup profiles and liquid flow fields
Li et al.[41]	3D, transient, two phase, Euler–Euler	Ø = 0.57 m sieve tray with flow-guided holes and bubble promoter; water/ air	Clear liquid height, liquid velocity distribution, liquid vector plots, streamlines and holdup distribution
Ping et al.[40]	3D, transient, two phase, VOF	Ø = 0.38 m sieve tray with 0-4° inclination; water/ air	Clear liquid height, liquid flow vectors and area of circulation
Malvin et al.[54]	3D, transient, VOF–LES	Ø = 1.21 m sieve tray; water/ air	Turbulent kinetic energy, clear liquid height, time-averaged liquid velocity profiles, droplet size distribution and mean sphere equivalent droplet diameter
Li et al.[55]	3D, steady state and steady–transient coupling, two phase, Euler-Euler	Elliptical (1.69 m x 0.85 m) and Ø = 1.2 m sieve trays; water/ air, and cyclohexane/ n-heptane	Clear liquid height, froth height, liquid and gas holdup distribution, liquid streamlines, liquid RTD, liquid phase molar fraction profiles and tray efficiency
Zarei et al.[42]	3D, transient, two phase, VOF-like method with MUSIG and SST model	Ø = 1.20 m conical cap (ConCap) tray; water/ air	Liquid volume fraction profiles, liquid and gas velocity vectors, total pressure drop and gas velocity variation along the height of cone

From the above model assessments, it can be easily observed that the majority of the hydrodynamic simulations are conducted for air-water system only, and validated with the experiments of Solari and Bell[26]. Even though large columns can have very different flow patterns than observed in the work of Solari and Bell[26]. This is still considered as the state-of-the-art for CFD validation irrespective of the recent experimental advances as mentioned in Tab 1. In addition, the clear liquid height is considered as the sole criterion for the validation of the CFD studies. Velocity distribution and other hydraulic parameters should be used for this purpose to certify confidence on the simulations. According to Schultes[45], the consideration of different correlations and empirical equations (e.g. to model interphase momentum exchange and coefficients for heat and mass transfer) leads to inconsistencies in the fluid dynamics, the separation efficiencies and the specific mass transfer area. Further, CFD results should correlate with the experiments as close as possible.[45] This is yet to be achieved for fluid dynamics due to which there is even more inconsistency in the tray efficiencies from experiments and simulations, because of the dependency of CFD models on standard mass-transfer rate equations and empirical approaches for mass-transfer coefficients.[47]

2.3 Objective Viewpoints

Despite of the concerns regarding mass transfer predictions, it is clear that CFD will be the part of the distillation modeler's toolbox in the near future to acquire the fluid dynamics on the trays. Therefore, a hybrid strategy is expected in the future considering CFD simulations to obtain the flow patterns and feeding them to mathematical models for efficiency predictions. The mathematical models were developed, based on phenomenological relationships, to associate the flow patterns and the liquid mixing with the tray efficiency. Since these models are an important prospect to account the tray performance, it is crucial to discuss their formulation, which would pave the way for their further evolution. To begin with the attributes of these models, some of them do not take the account of non-ideal flow on tray efficiency despite of several attempts

regarding the measurement and simulations of flow non-uniformities. Instead, they simply assume uniform liquid flow superimposed with mixing mechanism, uniform vapor flow with complete mixing between the trays, linear equilibrium curve and so forth. As stated earlier, the uniform flow of homogenous vapor is only possible between small diameter trays.[7] On large trays, however, hydraulic gradients produce serious non-uniform vapor distributions.[57] Besides, few of these models were formulated for rectangle-shaped trays.[58] The tray geometry, nevertheless, plays a big role in shaping the flow on trays. The curved walls near the downcomer create the tendency of directing liquid towards the tray centerline. This channeling causes the flow to separate under certain conditions, thus, creating re-circulatory patterns.[28] In addition, Lockett and Safekourdi[20] concluded that large deviations from the ideal velocity profile could be tolerated for small to medium diameter trays without significant loss in efficiency as long as stagnant regions are eliminated. The development of new or the modification of existing models to address and verify these possibilities is inevitable. Therefore, it is highly important to revisit and comparatively analyze the formulation of the existing tray models with their strengths and weaknesses. Recently, Taylor[47] also emphasized the need for understanding the formulation and solution of the model equations.

The present work intends to congregate the existing efficiency prediction models so that their characteristics can be discussed all-in-one place. A three-dimensional categorization of the available models, based on tray resolution (in terms of mathematical segmentation), liquid mixing and flow fields is presented in Fig. 4. Some models consider the whole tray while some segment the tray into channels and cells (pools) for material balancing. Flow patterns in terms of velocities and stream functions are also incorporated in few models. The degree of liquid mixing on a tray is specified on the third axis. An appropriate model should take incomplete liquid mixing into account and hence, must lie between the extreme points of this axis. On the other hand, an ideal model would be one that incorporates flow and mixing patterns at the best possible resolution to predict the Murphree tray efficiency accurately. Furthermore, most of the models

were formulated for liquid dispersion in the flow direction only. This classification allows an easy interpretation of the model categories and is prepared out of authors' perception.

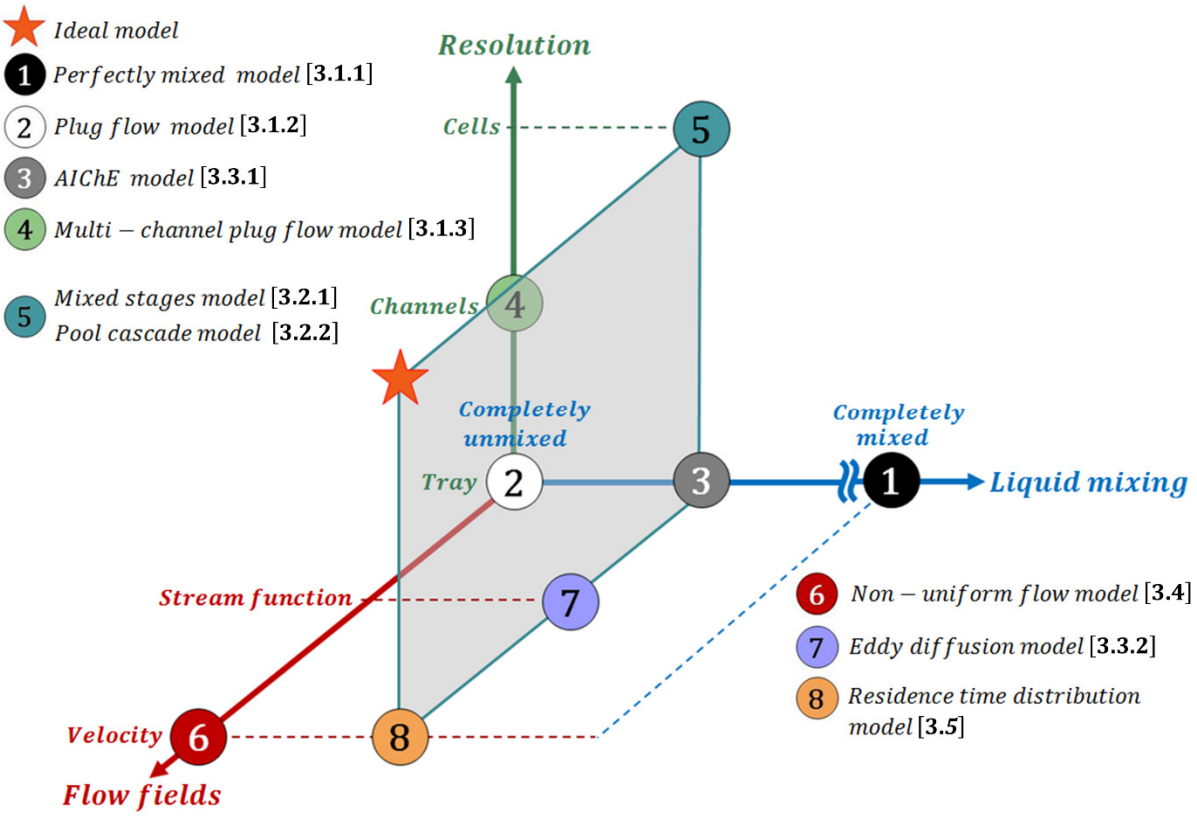

Fig. 4. Classification of tray efficiency prediction models.

3. Modeling Methodologies of Separation Efficiency

The mathematical models are categorized hereinafter based on the flow and the mixing of liquid on the tray. The first category comprises of the basic tray models that introduce the perfectly mixed and the plug flow of the liquid on a tray. The second category includes the pool models that describe the liquid mixing through perfectly mixed stages in the flow direction. The diffusional models form the third category, where liquid mixing is considered via eddy diffusion mechanism. The next category comprises of the non-uniform flow model that relates the non-ideal flow profiles, in the absence of liquid mixing, with the tray efficiency. Lastly, the residence time distribution (RTD) model describes the flow and the mixing patterns through liquid RTD

and evaluates their effect on the tray separation performance. Further description about these models is discussed henceforth.

3.1 Basic Tray Models

3.1.1 Perfectly Mixed Model

During the early 20th century, liquid on the tray was believed to be perfectly mixed due to the agitating action of vapor rising through shallow pool of moving liquid. This assumption implies the existence of a uniform liquid composition field. The vapor exiting the tray would also have uniform composition for perfectly mixed vapor entering the tray. These viewpoints lead to

$$E_{MV} = E_{OG} \quad . \tag{4}$$

However, in 1934, Kirschbaum[59] observed gradients in the liquid composition on a small tray (only few inches in diameter) at high superficial gas velocities. These findings led to the development of tray models enlisted below.

3.1.2 Plug Flow Model

Lewis[60] firstly introduced the concept of plug flow on distillation trays. In this model, liquid is assumed to travel across a rectangular bubble-cap tray without being mixed in the flow direction; however, there may be transverse mixing to any extent. The other assumptions are uniform liquid and vapor loads, linear vapor-liquid equilibrium curve and constant point efficiency throughout the tray. The material balancing over the tray yields the mathematical equations to predict the tray efficiency given in Tab. 3 for three different cases according to the liquid flow direction. These are the maximum achievable tray efficiencies for each case[3]. The efficiencies, in

actual, are lower due to the presence of mixing and non-uniformities in the liquid and the vapor flow.[3]

Tab. 3. Description of Lewis' plug flow model (⟶ liquid flow, ⇢ vapor flow).

Cases	Description	Model
(I) Vapor entering the tray is completely mixed.	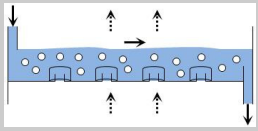	$E_{MV} = \{exp(\lambda E_{OG}) - 1\}/\lambda$ (5) λ is called stripping factor and is defined as $\lambda = b \cdot G/L.$ (6)
(II) Unmixed vapor rises upwards, while liquid flows in the same direction on successive trays.	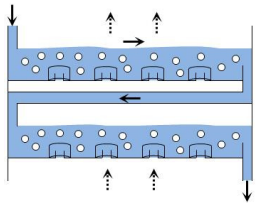	$E_{MV} = (\gamma - 1)/(\lambda - 1)$ (7) $\lambda = \left(\frac{1}{E_{OG}} + \frac{1}{\gamma - 1}\right) ln\, \gamma$ (8)
(III) All situations are identical to Case II except alternating flow of the liquid on successive trays.	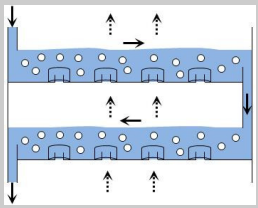	$E_{MV} = (\gamma - 1)/(\lambda - 1)$ (7) For $\gamma < 1$: $\lambda = \sqrt{\frac{\gamma^2 - (1 - E_{OG})^2}{{E_{OG}}^2(1 - \gamma^2)}} \cos^{-1}\left\{1 - \frac{(1 - \gamma)(\gamma - 1 + E_{OG})}{\gamma(2 - E_{OG})}\right\}$ (9) For $\gamma > 1$: $\lambda = \sqrt{\frac{\gamma^2 - (1 - E_{OG})^2}{{E_{OG}}^2(\gamma^2 - 1)}} \cosh^{-1}\left\{1 + \frac{(\gamma - 1)(\gamma - 1 + E_{OG})}{\gamma(2 - E_{OG})}\right\}$ (10)

Fig. 5 illustrates the tray efficiency for each case graphically. Here, the efficiency is highest in Case II, followed by Case I and III, for the given values of λ. This is because the counter-current nature of contact between liquid and vapor phase is maximum during Case II, intermediate during Case I and minimum during Case III.[3] However, since liquid flowing in the same direction on successive trays is uncommon,[3] as shown in Case II, Case I is the most often used approach for efficiency predictions.[3]

The models discussed so far demonstrate the two extremes of liquid mixing on a tray. As already stated, it is impossible to achieve the efficiency predicted by them due to incomplete or partial

mixing of the liquid in reality. However, they provide an encapsulation of the separation efficiency, presented as a grey shaded area in Fig. 6, within which the efficiency of a tray with real flow and mixing conditions should always be.[61] Strictly speaking, this holds only for the condition of completely mixed incoming vapor (i.e. uniform composition). Further, the intent of a distillation tray design should always be to approach the top (continuous) curve in Fig. 6, otherwise the tray would not fractionate as per expectations.

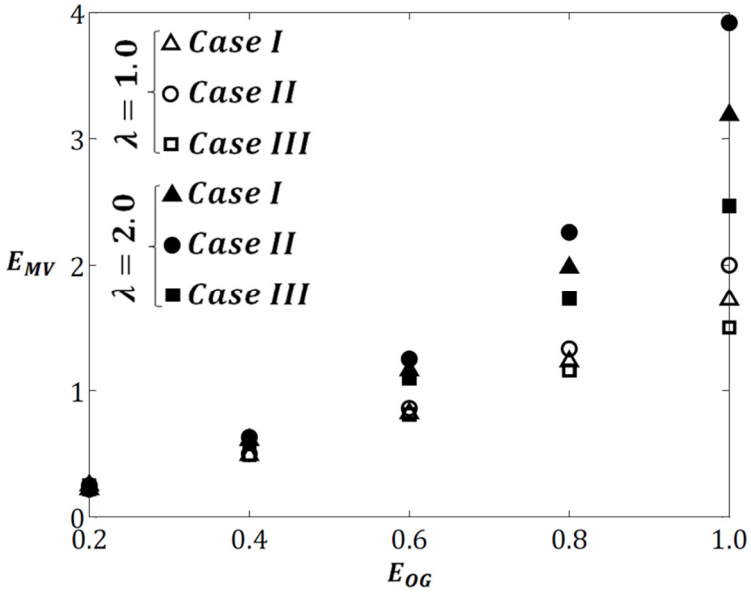

Fig. 5. Tray efficiency for the plug flow model.

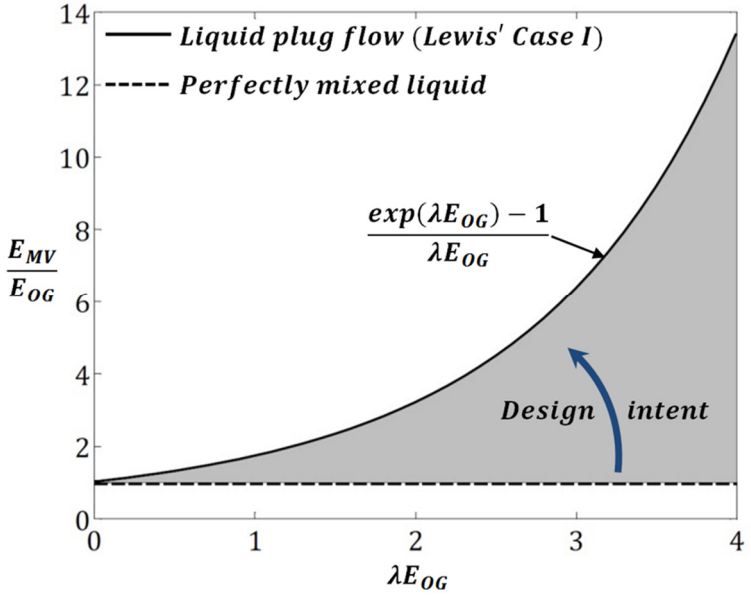

Fig. 6. Tray efficiency for perfectly mixed liquid and plug flow.

3.1.3 Multi-channel Plug Flow Model

Stichlmair and Ulbrich[10] observed channeling through distribution of liquid isotherms on bubble-cap and sieve trays. To account for liquid channeling in this model, the tray is assumed to consist of a large number of parallel channels, as depicted in Fig. 7. Plug flow behavior is assumed in each channel with different flow rates in accordance with the channeling profile. This assumption allows employing the Lewis' Case I to calculate the Murphree efficiency for each channel. This efficiency and the mass balance permit to find the liquid composition exiting each channel, for a given inlet composition. The averaging of the liquid composition from all channels enables to compute the tray efficiency.

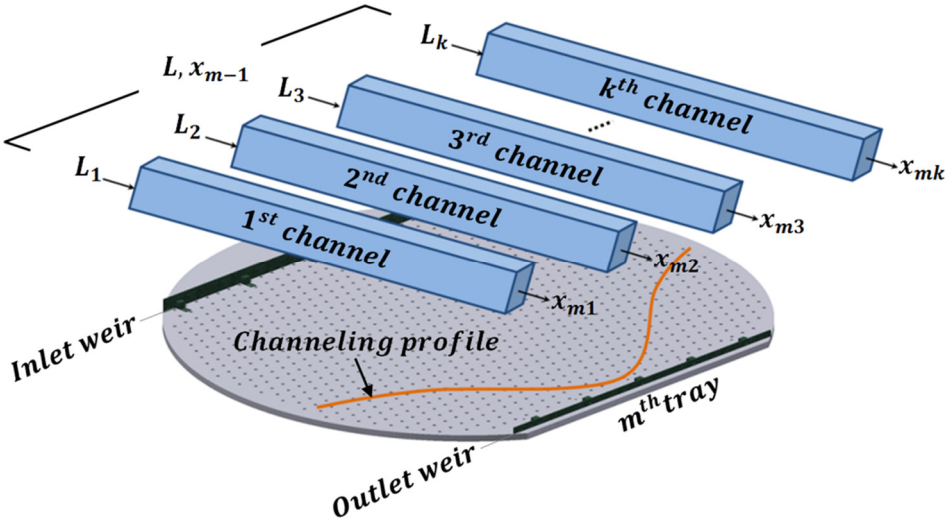

Fig. 7. Stichlmair's multi-channel plug flow model.

The maldistribution factor, defined as

$$MDF = \frac{1}{L_{mean}} \sqrt{\frac{1}{k-1} \sum_{i=1}^{k} (L_i - L_{mean})^2} \quad , \tag{11}$$

was devised to correlate the consequence of channeling with the tray separation performance. It would be appropriate to call this factor as the coefficient of variation, as termed by Olujic´ et al.[62] for the packed columns. In fact, this factor represents the normalized variation of the local liquid flow and approaches zero for the plug flow situation. The efficiency according to the experi-

mental data, obtained by Stichlmair and Ulbrich[10], is shown as the gray patch in Fig. 8. This figure depicts the effect of channeling on the tray efficiency, from which it can be inferred that the tray performance suffers greatly in case of severe channeling. However, the straight relation between the MDF and the tray efficiency is not explained in the literature.[10] Although this approach allows capturing the effect of channeling, the application of this method for the non-idealities other than liquid channeling is disputable.

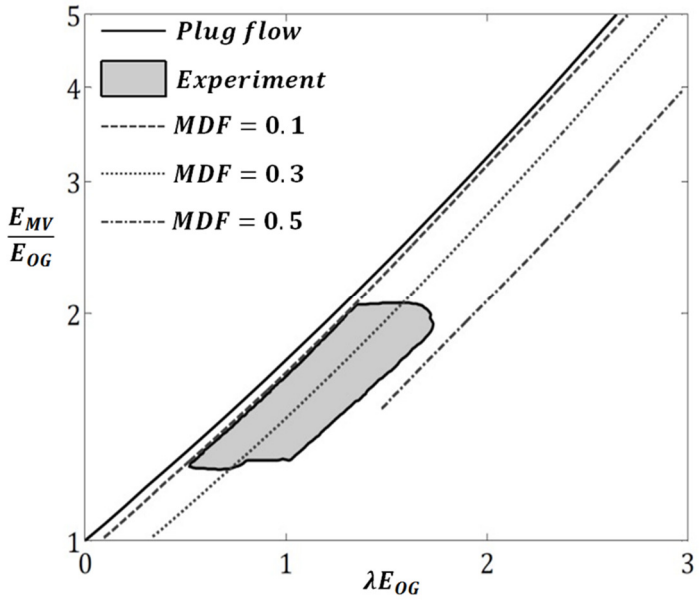

Fig. 8. Effect of channeling on tray performance for multi-channel plug flow.

3.2 Liquid Pool Models

Kirschbaum[63] firstly proposed a model that considers the tray consisting of several identical pools of completely mixed liquid. These pools account for liquid concentration gradients in the flow direction. The liquid is assumed to flow through the pools one-by-one from inlet to outlet weir. A tray with one pool and with an infinite number of pools can easily explain the limiting cases of perfectly mixed and unmixed liquid, respectively. An intermediate number of pools correspond to incomplete or partial mixing of liquid.

3.2.1 Mixed Stages Model

Gautreaux and O'Connell[64] employed the Kirschbaum's idea of perfectly mixed stages on separation trays. They revisited the mixed pool concept and derived the equation

$$E_{MV} = \left[\left(1 + \frac{\lambda E_{OG}}{n}\right)^{n} - 1\right]/\lambda \tag{12}$$

for n number of pools through material balancing on each stage (see Fig. 9), using the assumptions similar to the Lewis' case I except for liquid mixing. The derivation of the tray efficiency is simple and can be found in this publication.[64] The utility of this model was validated for the data obtained from a natural gasoline fractionator[65] (propane-butane system).[64]

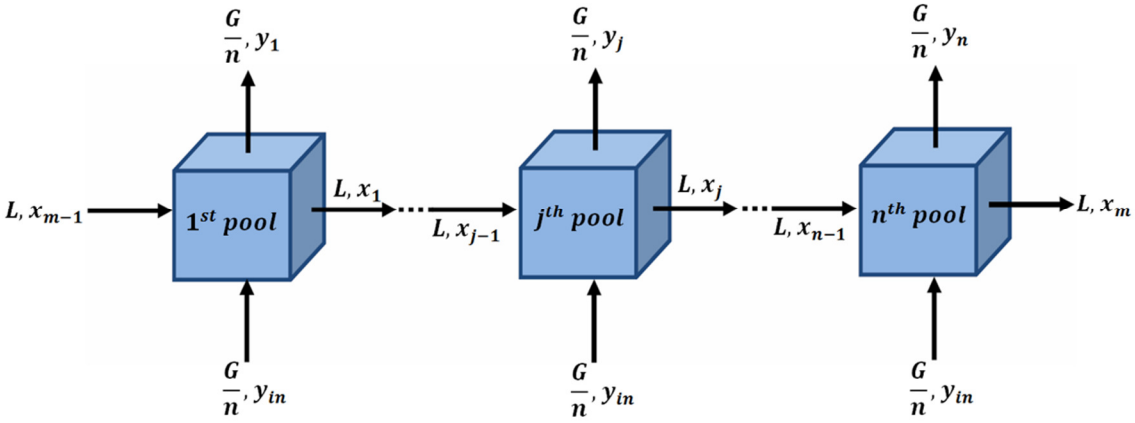

Fig. 9. Schematic representation of the pool model with perfectly mixed liquid pools.

Fig. 10 presents the tray efficiency according to Eq. 12. A significant growth in efficiency with increase in n can be noticed. This observation holds for lower values of n, where the intensity of the efficiency rise is proportional to λE_{OG}. The tray efficiency reaches maximum with further increase in n and becomes stable thereby approaching the plug flow. This figure shows the transition of the tray efficiency from the perfectly mixed liquid to the plug flow situation on the tray. For a fixed n, the gain in tray efficiency with increasing λE_{OG} is also evident. This observation is explained in Section 3.2.2.

Initially, the determination of the number of pools equivalent to the actual liquid mixing in the flow direction was unclear. Miyauchi and Vermeulen[66] identified the mathematical analogy be-

tween the axial dispersion model and the pool model assimilating backmixing amidst two consecutive pools.[67] The parameters for quantifying the liquid mixing are Péclet number (Pe) and number of pools in the dispersion model and the pool model, respectively. Pe and n denote continuous and discrete mixing in the respective methods. Further, Ashley and Haselden[68] confirmed that the axial dispersion and the pool model are equivalent for

$$Pe = 2(n-1), \text{ for } Pe > 2 \text{ and } \lambda E_{OG} < 0.5 \tag{13}$$

$$\text{and } Pe = 2n - 1 \text{ for large } Pe. \tag{14}$$

These observations were crucial for further developments in the pool modeling approach.

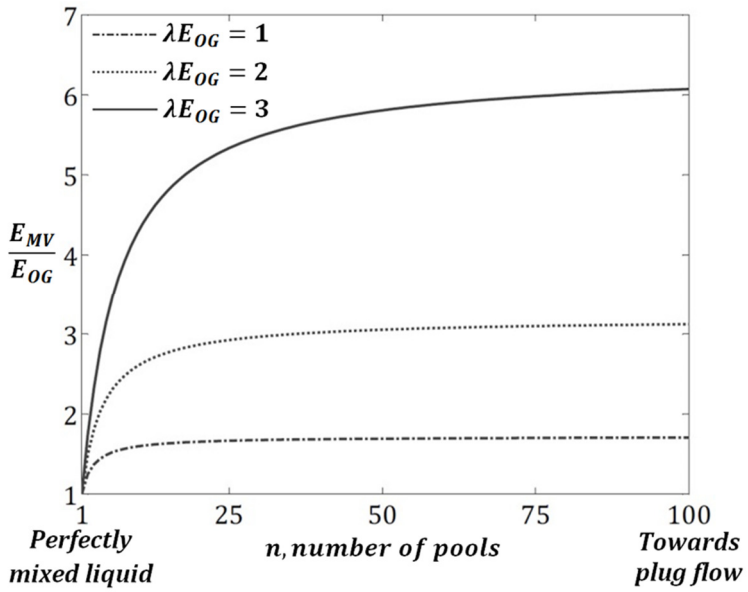

Fig. 10. Tray efficiency versus number of stages for the pool model.

3.2.2 Pool Cascade Model

Bruin and Freije[67] formulated a simple and versatile 'ready-to-use' model to incorporate the effects of channeling and stagnant regions on the tray efficiency. Here, the term versatility refers to the applicability of this method to a single-pass cross-flow tray of any design. This approach assumes the tray to be comprised of a cascade of identical mixing cells called main line mixers. This is different to Kirschbaum's concept, as each cell has a stagnant region in the form of a side

mixer connected to it. The main line mixers and the side mixers correspond to the active and the stagnant regions on the tray, respectively. According to Porter et al.[21], the stagnant regions are that part of the froth or spray bed, where the flow is either stationary or circulating with closed streamlines, while those regions lying in the liquid flow path are termed as active regions.

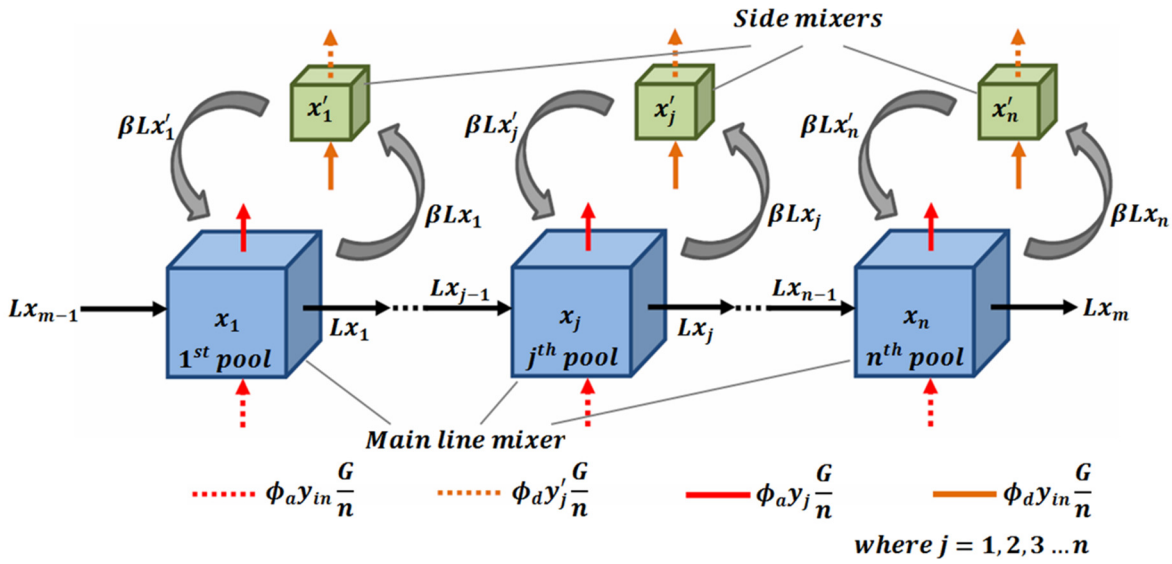

Fig. 11. Schematic representation of the pool cascade model.

With reference to Fig. 11, the comprehensive detailing of liquid flow on the tray can be observed. This is a necessity to incorporate the active and stagnant regions in this model. Comparatively, the vapor flow is not similarly detailed as its average composition is considered here. The loss of information because of these simplifications is compensated by the introduction of parameters such as size of the active and the stagnant regions, and the exchange of liquid between main line and side mixers. Fig. 11 illustrates the working concept of this model. Liquid (L) flows through a cascade of main line mixers. A fraction of this liquid (β) is exchanged between the main line mixer and its associated side mixer before passing on this liquid to the successive mixers. The information on the relative volume of these mixers is reduced to their relative areas (ϕ_a and ϕ_d, i.e. $\phi_a + \phi_d = 1$) due to the assumption of uniform froth height over the tray. The entry of the vapor proportional to the size of the corresponding mixer, constant point efficiency in each cell and linear VLE curve for an expected composition range are the other assumptions.

429 The mathematical modeling starts with the material balance in each cell. This enables to calcu-
430 late the average vapor composition leaving the cells, which is compulsory to predict the tray
431 efficiency. The material balance on j^{th} mixers provides the following equations

Main line mixer: $$L(x_j - x_{j-1}) + \beta L(x_j - x'_j) + \frac{G}{n}\phi_a(y_j - y_{in}) = 0 \quad (15)$$

Side mixer: $$\beta L(x_j - x'_j) + \frac{G}{n}\phi_d(y_{in} - y'_j) = 0 \quad . \quad (16)$$

432 The definition of the point efficiency provides important relationships for the j^{th} mixers as

Main line mixer: $$y_j = mE_{OG}x_j + (1 - E_{OG})y_{in} \quad (17)$$

Side mixer: $$y'_j = mE_{OG}x'_j + (1 - E_{OG})y_{in} \quad . \quad (18)$$

433 The average vapor composition exiting the tray can be obtained by using Eqs. 17 and 18 as

$$y_m = y_{in}(1 - E_{OG}) + mE_{OG}\phi_a \left\{ \sum_{j=1}^{n} \left(x_j + \frac{\phi_d}{\phi_a} x'_j \right) \right\} / n \quad . \quad (19)$$

434 By solving Eqs. 15 to 18 recursively followed by using Eq. 19 and the assumption of linear vapor-
435 liquid equilibrium, the tray efficiency can be formulated as

$$E_{MV} = \left[\left[1 + \frac{\lambda E_{OG}}{n} \left\{ \phi_a + \phi_d / \left(1 + \frac{\lambda E_{OG}\phi_d}{n\beta} \right) \right\} \right]^n - 1 \right] / \lambda \quad . \quad (20)$$

436 Since λ, E_{OG} and n are usually known from system properties and mass transfer/residence time
437 distribution correlations, ϕ_d(or ϕ_a) and β are the only adjustable parameters in the above equa-
438 tion.[67] The tray efficiency in Eq. 20 accounts for liquid channeling and stagnant zones through
439 these parameters. Further, the validity of Eq. 20 can be ensured by analyzing its transformation
440 for the limiting cases of liquid mixing. For a tray with completely mixed liquid, i.e. with just one
441 pool, β becomes infinitely large for a single cell due to which Eq. 20 transforms to Eq. 4. On the
442 other hand, β is zero for plug flow, which changes Eq. 20 to

$$E_{MV} = \left[\left(1 + \frac{\phi_a \lambda E_{OG}}{n}\right)^n - 1\right]/\lambda \quad . \tag{21}$$

An infinite number of cells correspond to liquid plug flow on a tray, which generates

$$E_{MV} = \left[exp(\phi_a \lambda E_{OG}) - 1\right]/\lambda \quad . \tag{22}$$

Appendix A describes the mathematical treatment on Eq. 21 to obtain the preceding equation. This was reported by Porter et al.[21] as the limiting solution for large trays without any liquid mixing. As far as the calculation of number of pools (Eq. 13) is concerned, it is advised to prefer the definition given by AIChE's bubble tray design manual[69] as

$$Pe = Z_1^2/(D_E \cdot \tau) \quad . \tag{23}$$

This is the general definition of Pe, thus, it can be used for any tray design, and hence maintains the model's versatility. Here, τ is the mean residence time of the liquid whereas D_E is the eddy diffusion coefficient that defines the amount of liquid backmixing on the tray. This coefficient depends on the flow characteristics and is influenced to a certain extent by the tray design.[70] Correlations for eddy diffusivity exist for a range of liquid and/or gas flow rates but are specific to the tray design. An accurate determination of Pe or D_E is inevitable for unambiguous efficiency calculations. The readers are referred to these publications[22,29,71-79] for further information on the degree of liquid mixing on trays.

Experiments and simulations regarding the flow visualization on trays are essential to this model as they can provide the relative size of active and stagnant regions (i.e. ϕ_a and ϕ_d). To derive β, the total exchanged flow between main line and side mixers is compared to the expected exchange between active and stagnant regions by eddy diffusion.[67] Besides, the volatile material transport to the rising vapor in a semi-infinite stagnant region is considered,[67] due to which the steady state penetration depth of the volatile component from active towards stagnant region is equivalent to the 'width of mixing zone'.[21] This comparison and the subsequent simplifications yield

$$\beta = \beta_o / \left\{ (1 + 0.5Pe)\sqrt{Pe} \right\} \quad . \tag{24}$$

The term β_o is an empirical fitting parameter and can be treated like a constant. This parameter can be calculated by using the above equation in conjunction with Eq. 20 for a system with known efficiencies. Bruin and Freije[67] recommended this parameter to be 4 as a first approximation and validated the accuracy of this model through experimental data (Zuiderweg et al.[80] and Gerster et al.[74]) and the eddy diffusion model[21] (discussed in Section 3.3.2). The current model is in good agreement with the Porter's model[21] but generally over-calculates the efficiencies by approximately 5-10% compared with the experimental data.

Considering the recommended value for β_o, Eq. 20 is illustrated graphically in Fig. 12 for the stagnant regions ranging from 10% to 50% of the tray perforated area. These results are presented using Eqs. 13 and 24 for the λE_{OG} values as 1 and 3. The prediction of the tray efficiency in absence of any stagnant region (i.e. Eq. 12) is also shown here. It can be concluded that the size of the stagnant region is inversely proportional to the tray efficiency. The larger is the size of stagnant regions, the more serious is the loss in efficiency.[21] For the given values of λE_{OG}, the efficiency loss is the highest for $\lambda E_{OG} = 3$. This inference is based upon the efficiency difference between no stagnant region and largest stagnant region curves for the corresponding values of Pe and λE_{OG}. Therefore, stagnant regions on the cross-flow trays should be eliminated as far as possible.

With reference to Eq. 23, the Péclet number is an indicator of the tray diameter as well as of the liquid mixing on the tray. Theoretically, high Péclet number corresponds to large-diameter trays as well as lower liquid mixing on them, and vice-versa.[21] Liquid mixing in the flow direction (i.e. backmixing) is adverse to the tray efficiency, whereas transverse mixing is favourable for the tray performance.[20] Furthermore, λE_{OG} depends on the system and has an influence on the cross-flow mixing on a tray.[21] Higher liquid mixing orthogonal to the flow direction can be expected for an increase in λE_{OG}. All these information may help in better interpretation of the graphical results.

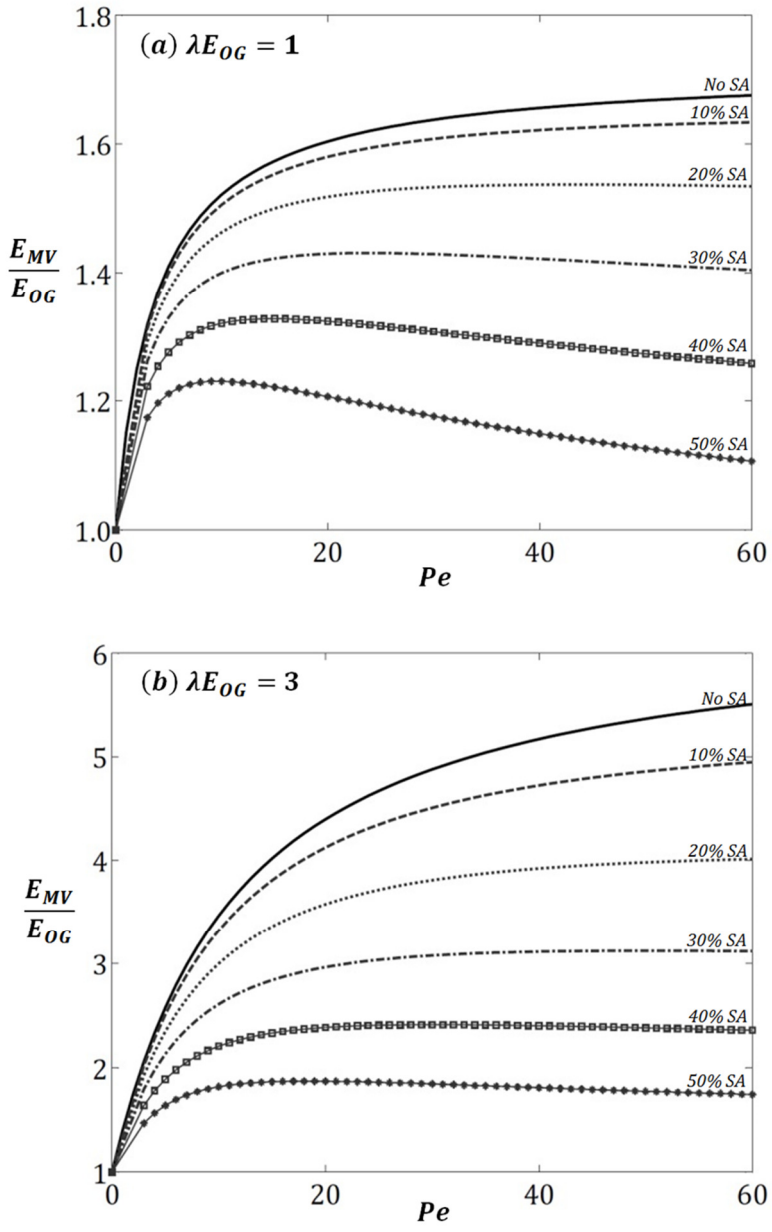

Fig. 12. Effect of channeling and dead zones on tray efficiency predicted by the pool cascade model for (a) $\lambda E_{OG} = 1$ and (b) $\lambda E_{OG} = 3$.

In Fig. 12, a sharp rise in the tray efficiency for low values of the Péclet number is visible. This means that transverse mixing of the liquid is dominant at this instant, which equalizes any flow non-uniformity on the tray.[20] In other words, the cross-flow liquid mixing on small trays is strong enough to wipe out the stagnant regions. This rise in efficiency with respect to the Péclet number becomes gradual and continues until the mixing in flow direction is less significant as compared to the transverse mixing. A further increase in the Péclet number refers to relatively larger trays, where the liquid cross-mixing is insufficient to deal with the flow non-idealities.

Due to this reason, large trays are susceptible to flow maldistribution and, therefore, no further improvement in the tray performance happens thereafter. The location of this point, where no improvement in the efficiency occurs, is dependent on the system and the flow parameters. The situation becomes supportive for the formation of stagnant regions as the Péclet number further increases. In addition to impeding the mass transfer, large dead zones can cause a significant amount of vapor bypassing, too.[21] These possibilities are evident in Fig. 12, where the tray efficiency eventually drops for the stagnant regions larger than 20% of the tray bubbling area. Furthermore, Porter et al.[21] emphasized the tendency of λE_{OG} to oppose the vapor bypassing. Thus, an increase in cross-flow mixing and higher resistance to vapor bypassing can be expected at higher λE_{OG}. These are the reasons behind improvement in the tray efficiency with increase in λE_{OG}. In addition, the position of the stagnant regions on large trays is also important. The majority of the mass transfer on such trays happens in their first half, near the inlet downcomer.[58] Therefore, the presence of any dead zone in the first half of a tray is highly disadvantageous for their separation performance.

Fig. 13 aims at providing information on the selection of the empirical parameter β_o (Eq. 24) for arbitrarily chosen values of Pe (10 and 40) and λE_{OG} (1). When Pe is 10, the maximum value of β_o is 18.9, for which β is marginally less than unity. For Pe equal to 40, β is far less than unity for the given range of β_o in Fig. 13b. The suggested value of this empirical parameter, i.e. 4 by Bruin et al.[67], appear to be valid for small stagnant regions. This is because no significant change is noticed in the efficiency after increasing this parameter. On the contrary, higher values of β_o are suitable for the efficiency predictions, where stagnant areas are larger.

The conclusive remarks about this model is that it is simple, versatile, ready-to-use and, is able to account for the effects of liquid channeling and stagnant regions on the tray efficiency. An improvement in this approach could be achieved by incorporating the effect of other non-uniformities in the liquid flow, such as retrograde flow and bypassing, as well as the location of dead zones on the tray fractionation performance. The determination of active and stagnant

regions on a cross-flow tray, through simulations or experiments, has to be precise for this model to perform satisfactorily.

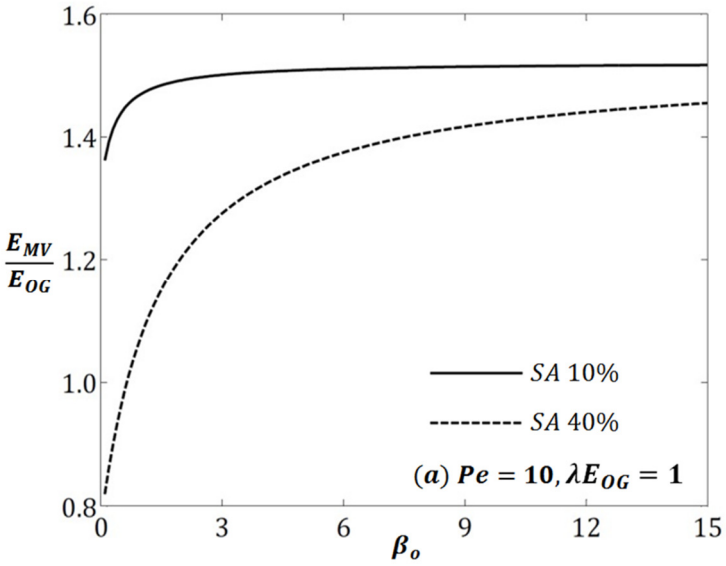

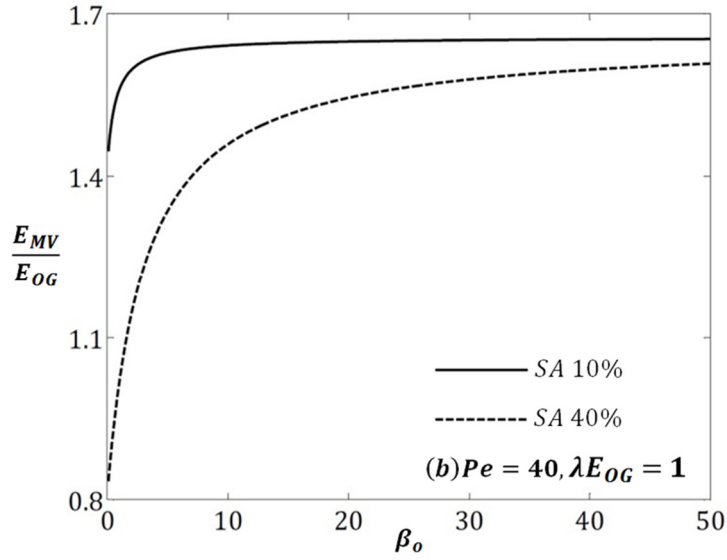

Fig. 13. Effect of the fitting parameter β_o on tray efficiency in the pool cascade model for (a) $Pe = 10$ and (b) $Pe = 40$, at $\lambda E_{OG} = 1$.

3.3 Diffusional Models

3.3.1 AIChE Model

The AIChE model is the most widely applied and accepted model to predict the tray separation efficiency. In this approach, liquid is assumed to be mixed by the eddy diffusion mechanism, akin to molecular diffusion.[74] The rate of mass transfer from one tray location to another is assumed being proportional to the concentration gradient in the flow direction.[74] The proportionality factor is called eddy diffusion coefficient, which has already been described in the pool cascade model in Section 3.2.2. This mixing happens in conjunction with the mass transport by bulk flow of the liquid across a tray.[74]

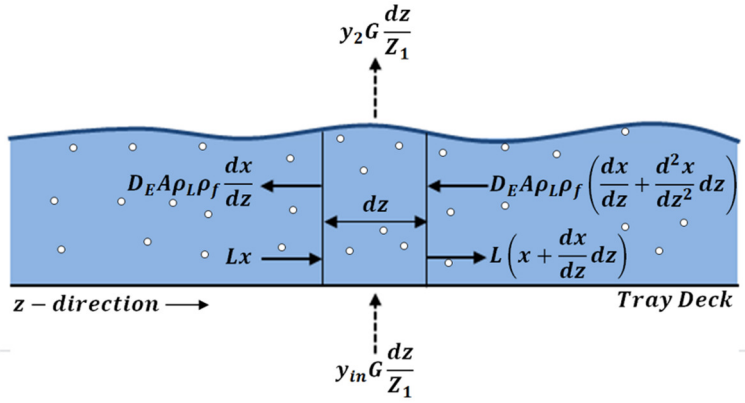

Fig. 14. Schematic representation of the AIChE model.

Although the concept of eddy diffusion is explained for a rectangular bubble-cap tray, it is extendable to the trays of other design, too. Firstly, liquid and gas-phase transfer units are required to find the point efficiency. Subsequently, they are used in a mathematical model to predict the tray efficiency. Constant point efficiency and linear VLE curve are the assumptions in this model. Fig. 14 shows the liquid plug flow on the tray upon which the backmixing is superimposed through eddy diffusion. The model starts with the mass balance on the vertical slice of the aerated liquid on the tray, which results in

$$D_E A \rho_L \rho_F \frac{d^2x}{dz^2} - L\frac{dx}{dz} - G\frac{(y_2 - y_{in})}{Z_1} = 0 \quad . \tag{25}$$

Given the average froth velocity as $V_f = L/(A\rho_L\rho_F)$, normalizing the distance from the inlet weir in the flow direction as $s = z/Z_1$, and modifying the point efficiency as $E_{OG} = (y_2 - y_{in})/(y_2^* - y_{in}) = (y_2 - y_{in})/\{m(x - x_e^*)\}$, Eq. 25 transforms to

$$\frac{D_E}{V_f Z_1}\frac{d^2x}{ds^2} - \frac{dx}{ds} - \lambda E_{OG}(x - x_e^*) = 0 \quad . \tag{26}$$

For convenience, the Péclet number in Eq. 23 is revised as $Pe = Z_1^2/(D_E \cdot \tau) = Z_1 \cdot (Z_1/\tau)/D_E = (Z_1 V_f)/D_E$. This simplifies Eq. 26 as

$$\frac{1}{Pe}\frac{d^2x}{ds^2} - \frac{dx}{ds} - \lambda E_{OG}(x - x_e^*) = 0 \quad . \tag{27}$$

The boundary conditions for the above equation are

$$x|_{s=1} = x_m \quad \text{and} \tag{28}$$

$$\left.\frac{dx}{ds}\right|_{s=1} = 0 \quad .^{81} \tag{29}$$

The second-order ordinary differential equation (Eq. 27) is solved in Appendix B for the given boundary conditions (Eqs. 28 and 29) and the final expression for the tray efficiency is

$$\frac{E_{MV}}{E_{OG}} = \frac{1 - exp\{-(\eta + Pe)\}}{(\eta + Pe)\left(1 + \frac{\eta + Pe}{\eta}\right)} + \frac{exp(\eta) - 1}{\eta\left(1 + \frac{\eta}{\eta + Pe}\right)} \tag{30}$$

$$\text{where} \quad \eta = \frac{Pe}{2}\left(\sqrt{1 + \frac{4\lambda E_{OG}}{Pe}} - 1\right) \quad . \tag{31}$$

Here, the tray efficiency depends on Pe and λE_{OG} only, out of which Pe requires an accurate determination of τ and D_E. As already mentioned in the pool cascade model, the eddy diffusion coefficient is influenced by the design of the tray.[70] The AIChE's report[74] gives a correlation of this coefficient for a rectangular bubble-cap tray; however, the flow patterns on circular trays can be very different than the idealized rectangular trays.[20] Further, the flow non-idealities are

566 the characteristics of circular trays, except those of very small diameter.[58] Therefore, it is ad-
567 vised either to find the diffusion coefficient experimentally or to calculate it from correlations,
568 for which the flow and the design parameters are within the range specified by the correlation.
569 The efficiency predictions of this model have been validated for a 5.5 feet bubble-cap trayed col-
570 umn (methyl dichloride – ethylene dichloride system).[69] The AIChE model agrees well with the
571 experimental efficiencies when they are below 100%, however, the predictions are over-
572 estimated, when the experimental efficiencies exceed unity.[69]

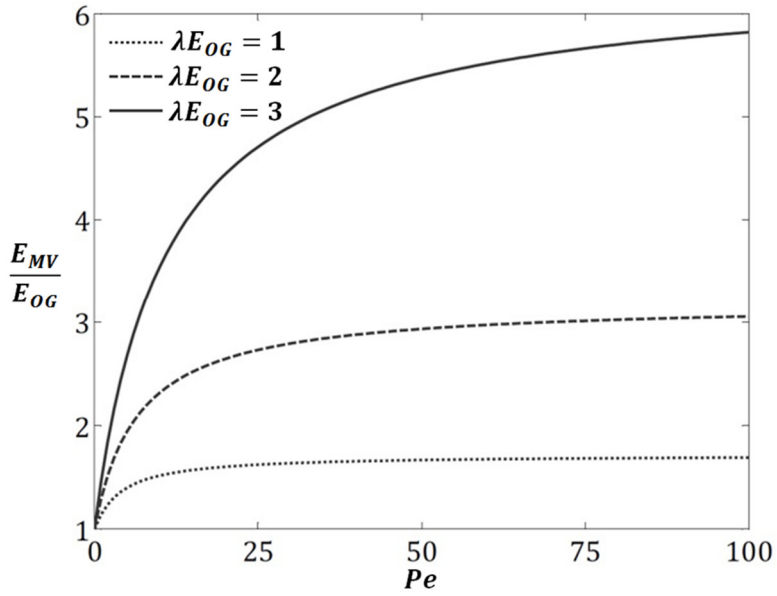

573

574 **Fig. 15.** Tray efficiency prediction using the AIChE model.

575 Fig. 15 illustrates the impact of Péclet number and λE_{OG} on the tray efficiency. The significance
576 of these non-dimensional parameters has been discussed in Section 3.2.2. A significant rise in
577 efficiency with Péclet number is apparent for the low values of Péclet number. This is because
578 the liquid mixing is significant on small trays, which eliminates the flow non-uniformities.[20] The
579 intensity of this efficiency rise, as mentioned in the Section 3.2.1, is proportional to λE_{OG}. Such
580 trend continues with increase in Péclet number until the liquid cross-mixing gets weaker and the
581 bulk liquid velocity becomes dominant for the material transfer.[20] This causes the efficiency to
582 rise with lower slope until it becomes constant.[20] The stagnation of tray efficiency is observable
583 in Fig. 15 for all values of λE_{OG} except for $\lambda E_{OG} = 3$, where the efficiency becomes stable at very

584 high Pe, which is beyond the range of this figure. Since the cross-flow effect enhances with in-
585 creasing λE_{OG}, it is straightforward to expect a higher efficiency for higher values of Pe and
586 λE_{OG}. However, large trays are susceptible to flow non-idealities, stagnant regions and eventual-
587 ly vapor channeling due to which the efficiency should not rise but rather fall. Since this model is
588 designed to account for the liquid backmixing only, it is insensitive to non-uniform flow profiles
589 and stagnant regions. This could be the reason behind the efficiency overprediction by this mod-
590 el during its validation. Hence, Porter et al.[21] named this model as 'simple backmixing model'.
591 Further, several authors have further claimed that this model overestimates the tray
592 efficiency,[21,58,67] which will be verified while comparing the results of the other models being
593 discussed. However, this model is still popular due to its simplicity and its ability to provide a
594 general estimate of the tray efficiency.

595

596 **3.3.2 Eddy Diffusion Model**

597 Porter et al.[21] and Lim et al.[82] developed the eddy diffusion model for single-pass and double-
598 pass cross-flow trays, respectively. These models account for liquid mixing in the flow direction
599 as well as in the transverse direction. Safekourdi[58] advanced these models by including liquid
600 velocities in terms of stream function over the bubbling area of the tray. The assumptions con-
601 sidered during the model formulation are

602 (i) constant point efficiency over the whole tray,
603 (ii) linear VLE curve for the expected composition range,
604 (iii) uniform liquid flow at the tray inlet,
605 (iv) completely mixed liquid and vapor entering the tray,
606 (v) perfect mixing of the liquid in the vertical direction in the froth, and
607 (vi) same eddy diffusivity in axial and transverse directions.

608 The coordinate system for a circular tray is shown in Fig. 3. Only half of the tray is considered
609 here due to symmetric concentration profiles on it.[26] An incremental area ($dz \cdot dw$) over the tray

having an aerated liquid (froth) with a uniform height h_f is considered. The transfer of mass into and out of this elemental froth is governed by the following mechanisms[58]:

(i) mass transfer due to bulk movement of the liquid across the tray,

(ii) mass transfer due to agitation of the liquid caused by the rising vapor, and

(iii) mass transfer from liquid to vapor.

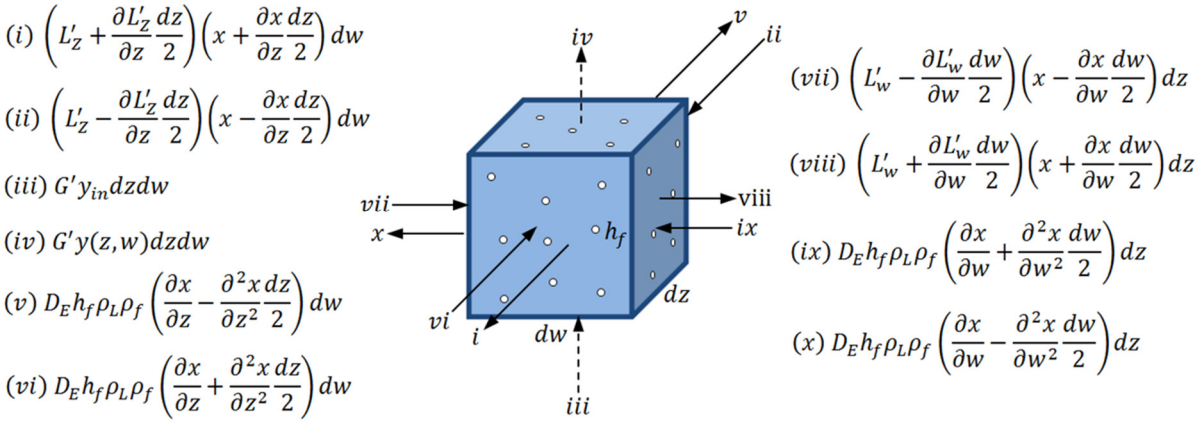

Fig. 16. Mass balance over the froth element on m^{th} tray.

The mass balance over the froth element, depicted in Fig. 16, leads to

$$D_E h_f \rho_L \rho_f \left(\frac{\partial^2 x}{\partial z^2}+\frac{\partial^2 x}{\partial w^2}\right)-L'_z\frac{\partial x}{\partial z}-L'_w\frac{\partial x}{\partial w}-x\left(\frac{\partial L'_z}{\partial z}+\frac{\partial L'_w}{\partial w}\right)-G'\{y(z,w)-y_{in}\}=0 \quad . \qquad (32)$$

Rearranging the above equation according to Appendix C gives

$$\frac{1}{Pe}\left(\frac{\partial^2 x}{\partial z'^2}+\frac{\partial^2 x}{\partial w'^2}\right)-\frac{W}{2D\psi_o}\left(\frac{\partial \psi}{\partial w'}\frac{\partial x}{\partial z'}-\frac{\partial \psi}{\partial z'}\frac{\partial x}{\partial w'}\right)-\frac{\lambda E_{OG} W D(x-x_e^*)}{A_b}=0 \quad . \qquad (33)$$

The boundary conditions for the liquid concentration and the stream function are

Centerline $$\frac{\partial x}{\partial w'}=0 \text{ and } \psi=0 \text{ at } w'=0 \text{ and } 0\le z'\le\frac{Z_1}{D}\ ; \qquad (34)$$

Inlet $$x_{+m}=x_{m-1}+\frac{1}{Pe}\frac{\partial x}{\partial z'},\frac{\partial \psi}{\partial z'}=0 \text{ and } \frac{\partial \psi}{\partial w'}=\text{constant at } z'=0 \text{ and } 0\le w'\le\frac{W}{2D}; \qquad (35)$$

Wall $$\frac{\partial x}{\partial \dot{n}}=0 \text{ and } \psi=\psi_o; \text{at } 0\le z'\le\frac{Z_1}{D} \text{ and } \frac{W}{2D}\le w'\le\frac{1}{2}; \qquad (36)$$

$$\text{Outlet} \quad \frac{\partial x}{\partial z'} = 0 \text{ and } \psi \text{ (shown graphically in Fig. 17); at } z' = \frac{Z_1}{D} \text{ and } 0 \leq w' \leq \frac{W}{2D} \quad . \qquad (37)$$

Eq. 33 is solved numerically with its associated boundary conditions using finite difference method. A detailed description on the finite-difference scheme, successive relaxation method and treatment of differentials near the wall are given in this publication.[58] Subsequently, the knowledge of the computed concentration profiles allows deriving the tray efficiency by following the treatment similar to Eqs. B8-B11 as

$$\frac{E_{MV}}{E_{OG}} = \left\{\frac{1}{A_b}\int_{A_b}(x - x_e^*)dA_b\right\} \Bigg/ \left\{\frac{1}{W}\int_{-W/2}^{W/2}(x_m - x_e^*)dw\right\} \quad . \qquad (38)$$

As per Eqs. 33 and 38, the tray efficiency is a function of liquid flow profile, Pe, tray design and λE_{OG}. The flow of liquid is assumed to vary linearly in the w-direction. The ratio of the liquid velocity at the wall and its mean value for any chord is denoted by q_s. Three values of q_s (0.5, 1.0 and 1.5) are considered to account for three different velocity profiles, as shown in Fig. 17. The stream functions corresponding to each profile have been calculated and supplied to Eq. 33. All previously stated equations in this model were solved numerically and the efficiencies obtained for different values of Pe are shown in Fig. 17. It is straightforward that the efficiency is highest during the chordal flow of liquid ($q_s = 1.0$). In addition, a uniform residence time distribution exists on a tray at $Pe = 200$ and $q_s = 1$ due to which the efficiency approaches the solution of Lewis' plug flow model.[60] This does not happen for the profiles corresponding to q_s values of 0.5 and 1.5.

As far as non-uniform flow patterns are concerned, the flow profile resembles the channeling for $q_s = 0.5$, i.e. having higher velocity at the tray centerline and lower velocity near the wall. This leads to stationary or deaccelerated regions close to the wall. Contrarily, no such possibility is anticipatable for $q_s = 1.5$ as near-the-wall velocities are larger than the centerline velocities. This could be a plausible explanation for higher efficiency in case of $q_s = 1.5$ than $q_s = 0.5$. Further, the computational ability and the validity of this model has been ensured by comparison

with the numerical solution of the AIChE[69] model. A slight overestimation of 3% in the efficiency required the predictions to be corrected by this value.[83] All results presented in this section have been corrected accordingly. The predictions from the model developed by Porter et al.[21] was another criterion for the model authentication.

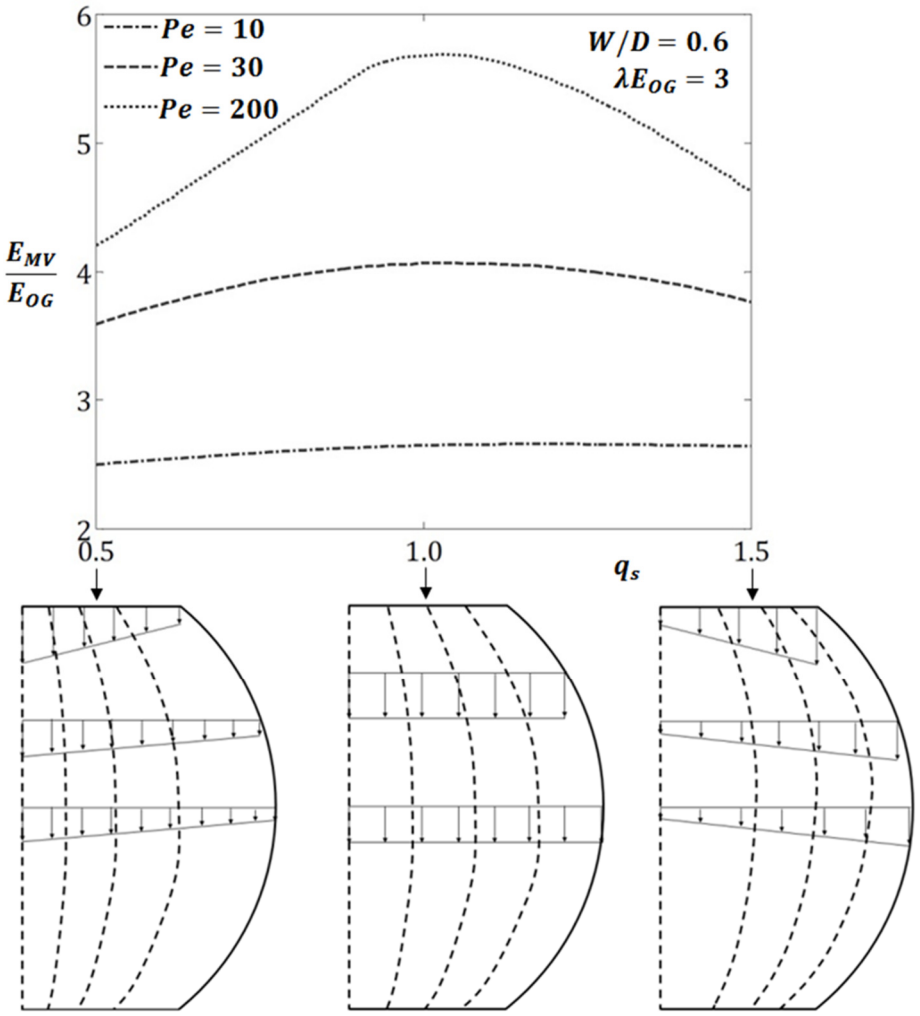

Fig. 17. Tray efficiency for three different velocity profiles (dotted lines on the halved trays represent the stream function for the corresponding velocity profile).

Fig. 18 shows the performance of the eddy diffusion model for the tray with uniform (optimal) liquid flow i.e. $q_s = 1.0$. The tray efficiency follows the same trend as in Fig. 15 due to similar reasons stated in Section 3.3.1. The calculation of the concentration profiles on a tray corresponding to the liquid flow profile and subsequent determination of the tray efficiency demands

plenty of computational effort. On the other hand, this remains the only model that considers liquid dispersion in the traverse as well as in the flow direction.

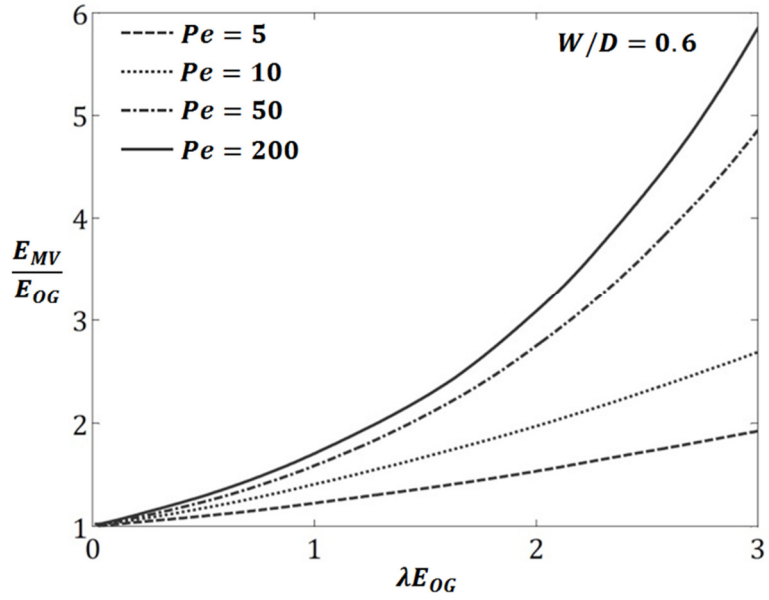

Fig. 18. Tray efficiency prediction for the optimum velocity profile by the eddy diffusion model.

3.4 Non-uniform Flow Model

The current model analyzes the effect of non-uniform velocity distributions, in the absence of liquid mixing, on the tray efficiency.[84] The absence of liquid mixing is essential to sustain a velocity profile throughout the tray. Although this concept is purely theoretical, it allows distinguishing between the effects of various flow patterns on the tray performance. The model considers two variations[84]: one for simple non-uniform velocities and the other for retrograde flow alongside non-uniform velocity distributions. For simplicity, a rectangular tray was assumed to derive the mathematical model. However, the model could be easily extended to circular tray geometries by increasing the flow path length near the wall.[84] No concentration gradients in the direction normal to the main flow have been assumed. The coordinate system of this model is given in Fig. 19a.

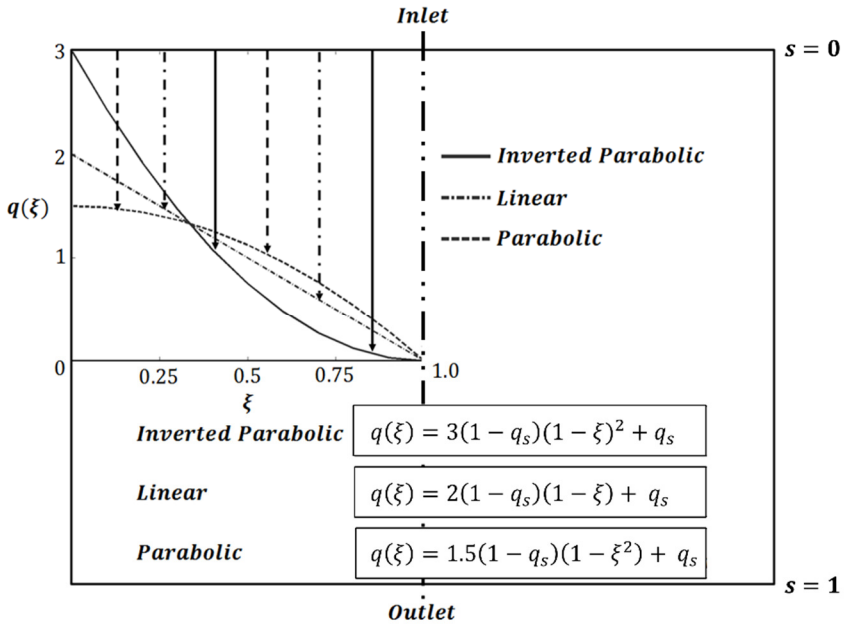

669

670 **(a)**

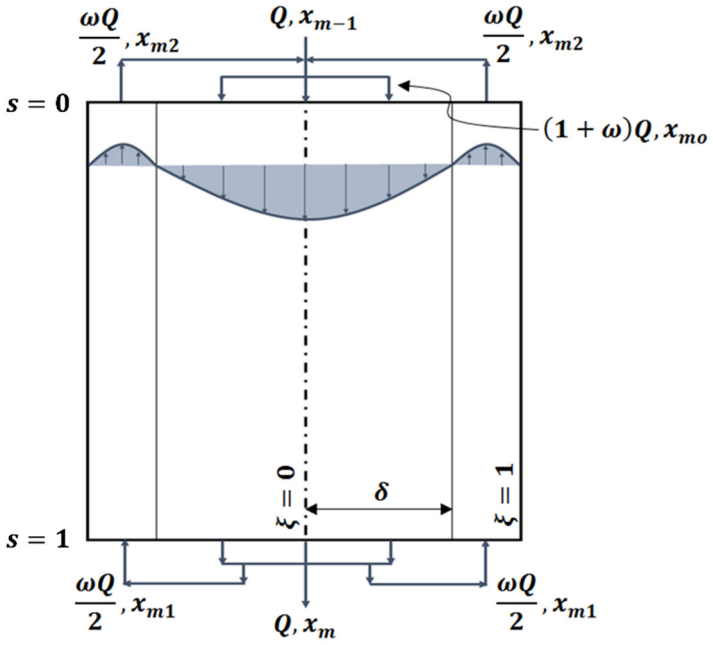

671

672 **(b)**

673 **Fig. 19.** (a) Co-ordinate system with velocity distributions for the simple non-uniform flow

674 model for q_s = 0 and (b) schematics of the retrograde flow model.

675 Bell[28] and Solari[83] reported the general mass transport equation for a binary system, derived

676 from the species continuity equation, as

$$q \cdot \nabla x - \nabla \cdot \left(\dot{P}e^{-1}\right) \cdot \nabla x - \lambda E_{OG}\{x_e^* - x(s,\xi)\} = 0 \quad . \tag{39}$$

This steady-state equation forms the basis of this model. The vector q is an arbitrary velocity field that is normalized by the average velocity corresponding to the uniform flow on the same tray and at the same flow rate. Uniform inlet vapor composition, linear VLE curve and constant λE_{OG} are the assumptions applied here. In addition, $\dot{Pe}$ is the Péclet number denoting the three-dimensional eddy mixing. It is taken as infinity due to the assumption of no mixing on the tray. This simplifies the above equation as

$$\frac{dx(s,\xi)}{ds} - \frac{\lambda E_{OG}}{q(\xi)}\{x_e^* - x(s,\xi)\} = 0 \quad . \tag{40}$$

Eq. 40 is solved for $x(s,\xi)$ by the method of separation of variables and subsequently used in the definitions of tray and point efficiency, which leads to

$$\frac{E_{MV}}{E_{OG}} = \left[\int_0^1 \frac{q(\xi)}{\lambda E_{OG}}\left\{1 - exp\left(-\frac{\lambda E_{OG}}{q(\xi)}\right)\right\} d\xi\right] \Big/ \left[\int_0^1 q(\xi)\left\{exp\left(-\frac{\lambda E_{OG}}{q(\xi)}\right)\right\} d\xi\right] \quad . \tag{41}$$

Three velocity distributions, namely inverted parabolic, linear and parabolic (see Fig. 19a) are analyzed here. The inverted parabolic distribution corresponds to severe channeling along the tray centerline, while the parabolic distribution closely resembles the uniform flow. q_s is the normalized slip velocity at the wall and is considered zero in Fig. 19a for simplicity. It is also a measure of intensity of the non-uniformity as shown by the equations mentioned in Fig. 19a.

Fig. 20 reveals the impact of these velocity distributions on the tray separation performance. Due to resemblance with uniform flow, the parabolic distribution seems more advantageous for the tray functioning than its counterparts. The efficiency-alleviating effect is the highest for the inverted parabolic distribution as it replicates severe liquid channeling on the tray. The efficiency of the linear distribution is intermediate between the other two profiles, as its flow intensity also lies amidst the other two distributions. This figure also confirms that a significant improvement in the tray efficiency with increase in λE_{OG} is only possible for uniform liquid flow, i.e. parabolic velocity distribution. Hence, the difference in the separation performance of these distributions is larger at higher values of λE_{OG}.

A peculiar observation about the inverted parabolic profile is that the E_{MV}/E_{OG} ratio at smaller values of λE_{OG} is less than unity for this distribution with a zero slip velocity at the wall. Foss et al.[73] also proclaimed the drop of the tray efficiency below point efficiency that approaches zero for bypassing liquid. This fact contradicts the possibility of the tray efficiency to fall between the mixing extremes on a tray, as shown in Fig. 6. However, in reality, this observation can be questioned as no such occurrence is reported in the AIChE analysis.[74] Besides, this model is one of the standalone methods that consider a liquid velocity profile at the tray inlet other than plug flow, as it can easily distinguish between the effects of these profiles on the tray performance.

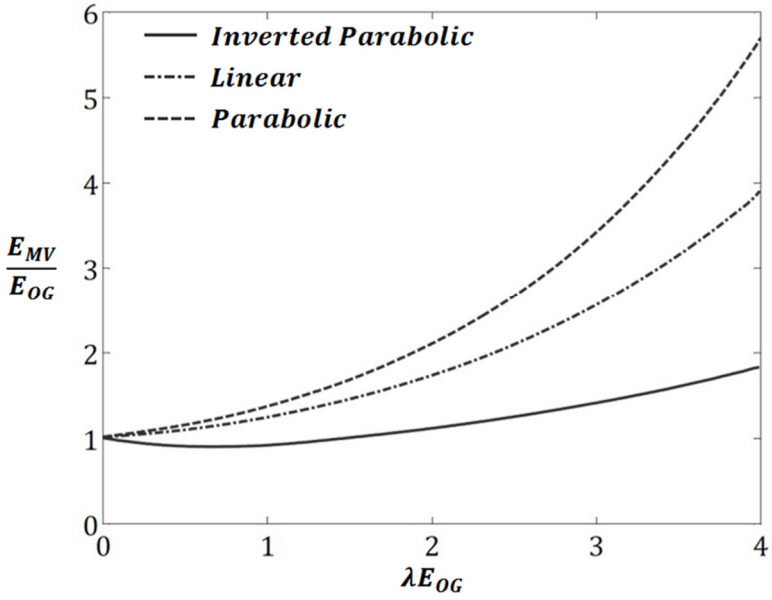

Fig. 20. Effect of different velocity profiles on tray efficiency from the non-uniform flow model.

Similar to the simple non-uniform flow model, Bell and Solari[84] devised another model by accommodating a retrograde flow on either side of the forward flow path, as demonstrated in Fig. 19b. The forward and the retrograde flow regions are separated by a line, where the liquid velocity is zero. This type of model has been termed as the 'non-uniform retrograde flow model' and is further classified into two sub-categories. In the first model, the liquid flowing through the forward flow path is perfectly mixed at the outlet. A fraction of this uniform composition liquid is diverted to the retrograde flow path and is called as 'uniform composition model' (as shown in Fig. 19b). In the second model (not shown here), some of the flow paths of the liquid near zero

velocity line are directly rotated to the retrograde flow region and is therefore named as 'external rotation model'. This causes the liquid near the tray centerline in the forward flow region to flow near the wall in the retrograde flow region. Here, the liquid composition varies across the inlet of the retrograde zone opposite to the uniform composition model. The expression of the tray efficiency for these cases can be derived by following a similar procedure as employed in the simple non-uniform flow model.[84]

3.5 Residence Time Distribution (RTD) Model

The RTD model employs the residence time concept to characterize the degree of liquid mixing on a tray. This method assumes that the mixing of liquid produces a distribution of residence time, ranging from zero to infinity.[73,85] This approach is capable of establishing the nature and the extent of all possible types of liquid mixing on various trays, indicating the superiority of this method over the existing models.

The concept of residence time is well-known and has been subjected to numerous studies in interdisciplinary fields.[86-88] Danckwerts[89] presented the unified and comprehensive treatment of this concept in continuous flow systems, after which the RTD studies gained large recognition and found application in chemical and reaction engineering. The experimental determination of the RTD based upon injection and dispersion of appropriate tracers, known as stimulus-response method, is discussed in detail in the literature.[90]

Fig. 21 shows the cross-flow of the liquid on the tray. The following assumptions are considered to formulate this model:

(i) liquid entering the tray consists of an infinite number of streams, each of which resides for a certain time on the tray,

(ii) plug flow of uniform gas through the liquid above the tray,

(iii) complete mixing of liquid in the vertical direction, and

742 (iv) linear VLE curve.

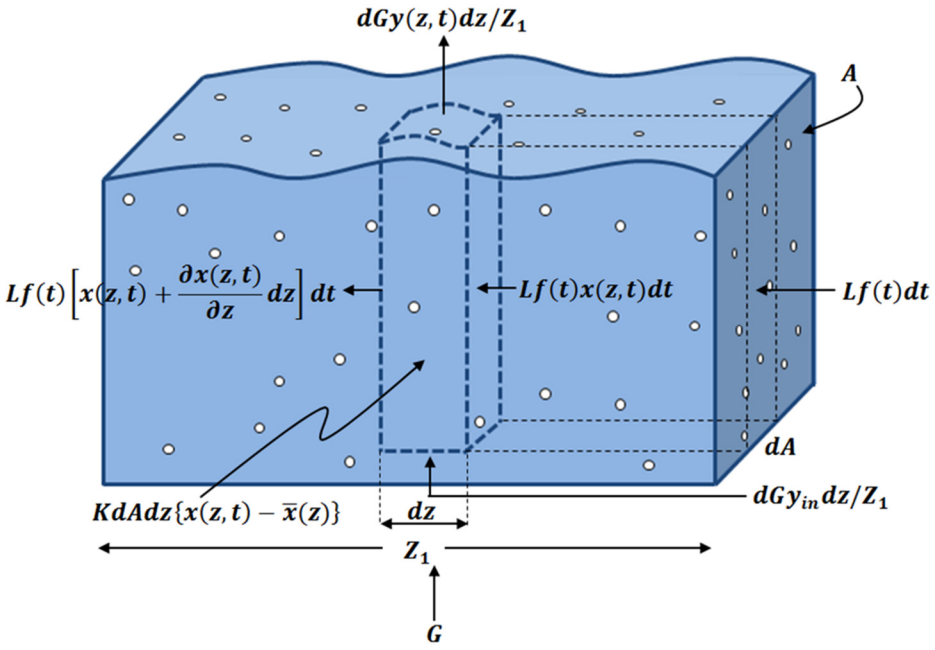

743

744 **Fig. 21.** Schematic representation of the RTD model.

745 The concentration of the dissolved material in each stream is affected by the mass transfer to the
746 gas at local efficiency and by exchange with its local surroundings.[85] A froth element residing on
747 the tray for a time ranging between t and $t + dt$ is subjected to the mass balancing. The total
748 material balance over the whole tray can be setup by summation over all fluid elements, if their
749 residence time distribution is known. Fig. 21 displays an aerated element with the cross-
750 sectional area dA and with a liquid stream $Lf(t)dt$. Here, $f(t)$ is the liquid residence time func-
751 tion that describes, how much time different fluid elements have resided on the tray quantita-
752 tively.[91] Using assumption (i), the residence time of each stream is given by

$$t \propto \frac{dA}{Lf(t)dt} \quad . \tag{42}$$

753 Similarly, the mean residence time of all streams is

$$\tau \propto \frac{A}{L} \quad . \tag{43}$$

Since the proportionality constant is the same in Eqs. 42 and 43, the fraction of the total froth volume on the tray occupied by a differential element is directly proportional to its residence time and the fraction of the total flow as

$$\frac{dA}{A} = \frac{t}{\tau} f(t)dt \quad . \tag{44}$$

Using the assumption (ii) and Eq. 44, one can obtain

$$\frac{dG}{G} = \frac{dA}{A} = \frac{t}{\tau} f(t)dt \quad . \tag{45}$$

The mass balance in the elemental volume ($dA \cdot dz$) located at point z (with reference to Fig. 21) results in

$$Lf(t)dt\left\{\frac{\partial x(z,t)}{\partial z}dz\right\} + dG\{y(z,t) - y_{in}\}\frac{dz}{Z_1} + KdAdz\{x(z,t) - \bar{x}(z)\} = 0 \quad . \tag{46}$$

The first two terms in the above equation describe the net mass transfer corresponding to liquid and gas flow, respectively, whereas the last term represents the intermixing of liquid owing to diffusion in the differential element. This intermixing is assumed to be proportional to the size of the fluid element. $\bar{x}(z)$ is the space-mean concentration at point z, which is defined as

$$\bar{x}(z) = \int_0^A x(z,t)\frac{dA}{A} = \int_0^\infty x(z,t)\frac{t}{\tau} f(t)dt \quad . \tag{47}$$

The mathematical treatment on Eq. 46 to obtain the tray efficiency is described in Appendix D, which results as

$$E_{MV} = \frac{1 - \int_0^\infty \exp(-\lambda E_{OG}\, t/\tau) \cdot f(t)dt}{\lambda \int_0^\infty \exp(-\lambda E_{OG}\, t/\tau) \cdot f(t)dt} \quad . \tag{48}$$

The procedure to calculate the point efficiency is briefly introduced in the AIChE model in Section 3.3.1. If the point efficiency is supposed to be constant, then the tray efficiency can be expressed as

$$\frac{E_{MV}}{E_{OG}} = \frac{1 - \int_0^\infty \exp(-\lambda E_{OG}\, t/\tau) \cdot f(t) dt}{\lambda E_{OG} \int_0^\infty \exp(-\lambda E_{OG}\, t/\tau) \cdot f(t) dt} \quad . \tag{49}$$

As mentioned previously, a cross-check is performed on the tray efficiency by analyzing the transformation of the model for completely mixed and plug flow cases. The residence time functions are available for the systems with completely mixed and unmixed liquid. By supplying these functions to Eq. 49, the efficiency for the respective cases of mixing is easy to obtain.[85]

The dependency of the tray fractionation efficiency on $f(t)$ and λE_{OG} is evident from Eq. 49. As far as previous tray models are concerned, liquid mixing in the flow direction is accounted by the Péclet number. Except for the eddy diffusion model,[21,58,82] no account of the Péclet number normal to the flow direction for transverse mixing has been observed. The absence of Péclet number in this model is automatically compensated by the residence time function, as it also recognizes the mixing in the flow direction. However, point tracer concentration measurements in stimulus-response experiments further enable to extract the flow patterns on the trays.[18,26-28] The correctness of this model has been justified through the oxygen-stripping studies[92] on a sieve tray unit operated with oxygen-rich water and air. The present model slightly over-predicts the efficiency (approximately 5%) due to non-uniform froth conditions at the liquid entrance.[73]

There is a severe lack of data concerning the residence time function of liquid on cross-flow trays. Foss et al.[73] conducted the tracer experiments on a rectangular sieve tray that was 36 inches long and 9.5 inches wide. A concentrated solution of salt was used as the tracer. A step input of the tracer was supplied to the liquid entering the tray. The tracer concentration in the effluent stream was measured continuously by a conductivity cell.[85] The residence time functions with their mean residence time at different load conditions are exemplarily presented in Fig. 22a.[73] The curve with the mean residence time of 15.7 s corresponds to liquid flow rate of 17.49 $cm^3/(cm{\cdot}s)$ and gas flow rate of 1.84 $m^3/(m^2{\cdot}s)$. Similarly, the curve with the mean residence time of 2.98 s corresponds to liquid and gas load of 90.04 $cm^3/(cm{\cdot}s)$ and 1.83 $m^3/(m^2{\cdot}s)$,

792 respectively. The liquid and gas flow rates are mentioned here with respect to the width and the
793 active area of the tray, respectively.

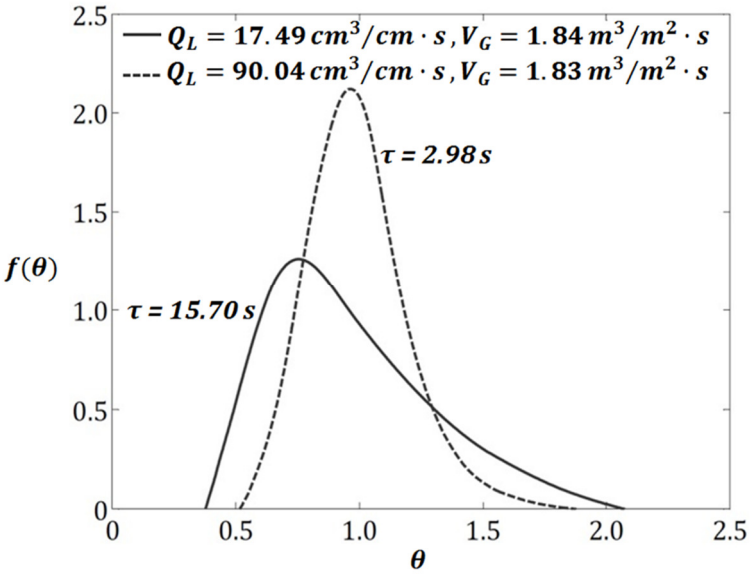

794

795 **(a)**

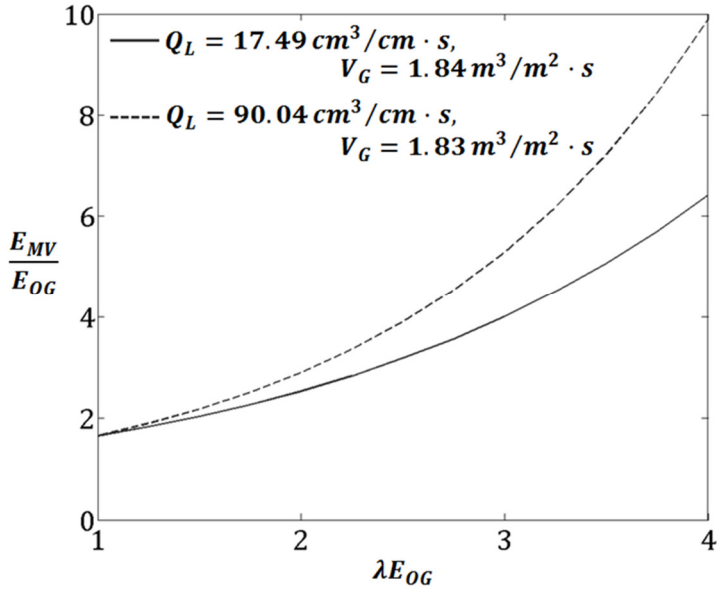

796

797 **(b)**

798 **Fig. 22.** (a) Residence time function at the tray outlet and (b) tray efficiency predictions by the
799 RTD model.

800 Since the time scale of these functions vary from each other, their comparison is only possible by
801 normalizing their time scale with the corresponding mean time. The occurrence of the lower

mean residence time at higher liquid flow rate and vice-versa at constant gas flow is obvious. The spreading of these curves denotes the level of liquid mixing on the tray in the flow direction. The higher the momentum of the liquid, the lower is its axial or longitudinal mixing. Apart from this, the position of the peak of these curves relative to their mean is very important for the diagnosis of the tray functioning. For instance, a distribution that peaks before its mean indicates the liquid short-circuiting or bypassing.[73] These functions are supplied to Eq. 49 to calculate the ratio of the tray and the point efficiencies at different λE_{OG}, as shown in Fig. 22b. This computation is intended only for highlighting the effects of flow and mixing patterns via distribution function on the tray efficiency. Further, the unavailability of the slope of the VLE curve forces to assume a certain value for λE_{OG} since the point efficiency is also supposed to be constant. The separation performance of the tray with higher liquid flow is better than the other case. This is straightforward as the tray with lower liquid flow undergoes liquid bypassing, as suggested by the peak position of the distribution. The E_{MV}/E_{OG} values for λE_{OG} less than unity are not shown here deliberately as these RTD functions are ineligible for these values of λE_{OG}. The difference in the performance of these two cases increases with λE_{OG}, which is consistent with results of the previous models.

A weak point of the RTD studies is that they are unable to uniquely determine the nature,[93] as well as the location of the non-ideality. Similar tracer response is possible for different non-idealities at different locations on the tray. However, this approach is the most realistic among the available models since it is unlikely that a number of perfectly mixed pools would actually exist on a tray.[73] Furthermore, the concept of eddy diffusion only holds, when there are large number of repetitions of the diffusive mechanism and, is incapable of handling extreme liquid bypassing.[73] The RTD model, however, is capable of addressing these possibilities. The feasibility of tracer-response experiments further makes this model a prominent choice for the efficiency predictions, especially in industry.

4. Comparison of Modeling Schemes

In order to compare the results of the existing models, the factors on which these models rely need to be considered. λE_{OG} and Pe appear in almost every model, while the other factors are weir length to diameter ratio,[58] relative size of active and stagnant regions,[67] liquid composition,[58] and residence time function.[73] This diversity in factors hinders the straightforward comparison of the models on a common ground. Thus, an attempt to collate the results from some of the existing methods at arbitrarily selected values of Pe for the usual range of λE_{OG} is demonstrated in Fig. 23a and 23b.

The plug flow [3.1.2] and the perfectly mixed [3.1.1] model provide the upper and the lower limits of the tray efficiency, respectively. The predictions by the mixed stages model [3.2.1] and the AIChE model [3.3.1] at $Pe = 50$ practically coincide. These models consider the liquid backmixing only and are unconcerned towards the stagnant regions due to which the results from the pool cascade model [3.2.2] at $\beta_o = 4$ are also presented. It is obvious that the size of the stagnant regions is proportional to the loss in the tray efficiency. The influence of λE_{OG} and Péclet number on the tray efficiency has been discussed several times in this work. However, this model comparison is only applicable for the tray assuming uniform liquid flow at the inlet. Apart from this, Bell and Solari[84] reported that the tray efficiency becomes less than the point efficiency for an inverted parabolic velocity profile of liquid at the inlet (see Fig. 20). The pool cascade model also provides similar observation (not shown here) e.g. the E_{MV}/E_{OG} ratio goes below unity for relative stagnant regions larger than 80% at $Pe = 5$.

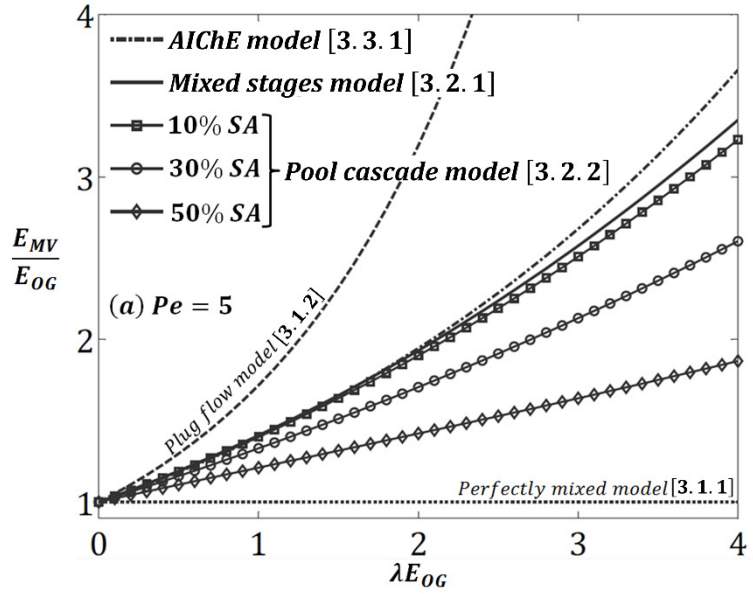

848

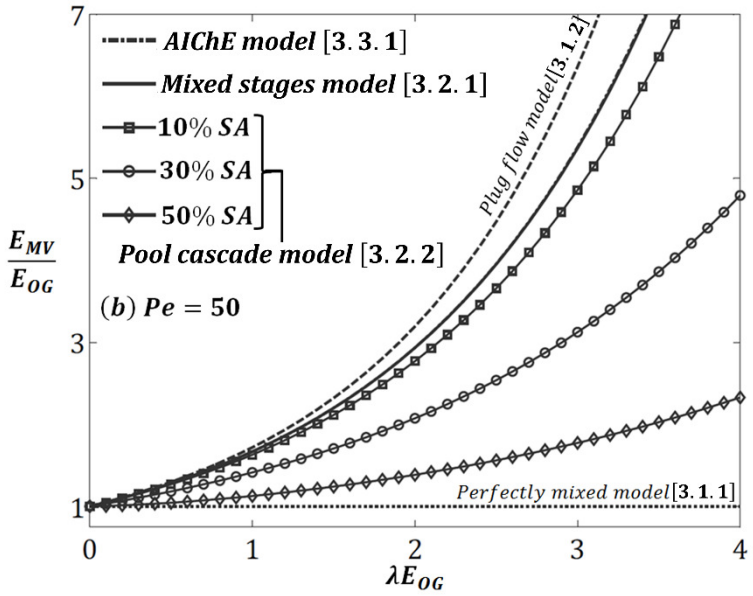

849

850 **Fig. 23.** Comparison of efficiency predictions from different tray models at (a) *Pe* = 5 and

851 (b) *Pe* = 50.

852 Furthermore, the tray models are summarized in Tab. 4 in terms of their ability to account for
853 flow and/or mixing patterns. Out of all models, the RTD model is the most realistic one as it is
854 capable of describing all types of liquid mixing in the flow direction on the tray. The point mean
855 residence time calculations further reveal the flow profiles on the tray. To make this model bet-
856 ter, it needs to be upgraded so that it can account for transverse mixing of the liquid and can
857 differentiate between the effects of different non-idealities on the tray efficiency. A significant
858 development in the tray efficiency modeling would be the inclusion of possible non-uniform

vapor distributions in the model formulation. Further, the 'Hybrid modeling' approach combining experimentally validated CFD and tray efficiency models seems to be a promising alternative for realistic efficiency predictions. Such hybrid approach could be preferred in the future as 'virtual experiment'[36] compared to real experiments which can be expensive and time consuming. Besides, the discussed models have been developed for non-reactive systems and hence, it would be interesting to modify the most prominent ones for the reacting systems.[9] Lastly, the tray efficiencies are calculated using the flow conditions at the tray boundaries, i.e. inlet and outlet, without giving any preference to the flow scenario at intermediate locations (except in the eddy diffusion model). This is similar to the treatment of distillation trays as black box. Therefore, an account of the intermediate flow conditions in phenomenological models for evolving tray efficiencies is another necessity.

Tab. 4: Summarization of existing tray models according to their respective account of flow patterns and liquid mixing on the tray. (✓ Acknowledged, ✗ Overlooked)

Model	Liquid mixing		Flow patterns	Remarks
	Flow direction	Transverse direction		
3.1.1. Perfectly mixed model		✓	✗	Considers uniform liquid composition over the tray
3.1.2. Plug flow model		✗		Predicts the maximum achievable efficiency
3.1.3. Multi-channel plug flow model		✗	✓	Accounts for liquid channeling only
3.2.1. Mixed stages model	✓	✗	✗	Sensitive to backmixing of liquid only
3.2.2. Pool cascade model	✓	✓	✗	Concerned towards channeling and stagnant zones
3.3.1. AIChE model	✓	✗	✗	Most popular; accounts for liquid backmixing only
3.3.2. Eddy diffusion model	✓	✓	✓	Most all-round model yet computationally expensive
3.4. Non-uniform flow model		✗	✓	Capable of distinguishing between the effects of velocity profiles on tray efficiency
3.5. RTD model	✓	✗	✓	Most realistic model to account for flow patterns and liquid mixing in the flow direction

5. From Experiments to Efficiency Predictions: A Roadmap

One obvious question that remain unanswered is that how to utilize the experimental studies for extracting the inputs required for the mathematical models. The stimulus-response method has been a popular choice to quantify the flow patterns in process equipments, and was preferred by Solari and Bell[26] and Schubert et al.[18], while using fibre-optic system and conductivity wire mesh sensor (WMS) respectively. The latter study is favored for the aforementioned purpose due to the availability of data at comparatively high spatial and temporal resolution. In this investigation, two sieve trays with 5% fractional open area were used in an 800 mm diameter column. A WMS, comprising of two orthogonal planes of transmitting and receiving wires, was embedded on one of the trays. The effects of liquid load and outlet weir design on the flow patterns were evaluated through the dispersion of salt (Na_2SO_4) solution used as the tracer. The virtual crossing points between axially separated transmitters and receivers in the WMS allow measuring time-dependent tracer concentrations, and hence point liquid residence time distribution. The readers are referred to Schubert et al.[18] for further details on column design, data calibration and flow visualization.

The distribution of liquid residence time represents the extent of flow non-idealities in a system. This distribution is opportune as its mathematical processing can lead to determination of the parameters needed in the described models. The point tracer concentrations need to be averaged at the tray boundaries to realize the RTD function according to

$$C_{out}(t) = C_{in}(t) \otimes f(t) \quad . \tag{50}$$

Here, $C_{in}(t)$ and $C_{out}(t)$ are the tracer concentrations that are mathematically averaged point concentrations for each time step at the tray inlet and outlet, respectively. In this work, the data from the WMS points next to the weirs are avoided to neglect the effect of non-uniform froth at the boundaries[73], as well as to account for the flow in the tray bubbling area only. These boundaries will be referred as WMS boundaries hereafter. Furthermore, the symbol $\otimes$ refers to the

convolution integral, whose calculation is straightforward.[90,94] The converse of this integral is called deconvolution, which is challenging and hence requires special approaches.[94] For this purpose, several techniques such as Laplace and Fourier methods, flow model fitting, simultaneous solution of linear equations, and others have been proposed in the literature.[90,94-108] The cited literature also explains the pros and cons of these techniques due to which they are not discussed here. The model fitting approach is preferred in this work, because of the computational ease due to the availability of the standard RTD function from the axial dispersion model. The WMS boundaries permit to use the Gaussian function for the open-open boundary condition[90,101,109] as

$$f(t) = \sqrt{\frac{Pe}{4\pi t \tau_h}} \cdot exp\left\{ -\frac{Pe\left(1-\frac{t}{\tau_h}\right)^2}{4\left(\frac{t}{\tau_h}\right)} \right\} \quad . \tag{51}$$

Here, τ_h is the time based on bulk liquid velocity and flow path length, and is called as hydraulic or space time. Before proceeding further, it is important to focus on the Péclet number in the above equation. Levenspiel[90] suggested to refer to this term as an inverse of the vessel dispersion number, and strongly objected the usage of the Péclet number. Still, Pe is being used here due to its popularity and wide acceptance in the chemical reactor engineering. Further, it has been defined in the literature[90,91] as

$$Pe = \frac{\text{Movement by bulk flow}}{\text{Movement by longitudinal dispersion}} = \frac{Z_1^2}{D_E \cdot \tau_h} \quad . \tag{52}$$

This generalized definition of Pe is apt for the open-open boundary condition. For the closed system, the mean residence time is the same as the hydraulic time.[90,91] This is an explanation for the appearance of the mean residence time in Eq. 23 as proposed in the AIChE manual[69].

The algorithm to obtain the tray RTD function is discussed concisely as following:

(i) Compute the response function at the WMS boundaries according to

$$R(t) = \frac{c(t)}{\int_0^\infty c(t)dt} \quad . \tag{53}$$

916 (ii) Assume the adjustable parameters, i.e. Pe and τ_h, in Eq. 51 and calculate the approx-
917 imate RTD function.
918 (iii) Convolute the inlet response and the RTD function leading to the convoluted func-
919 tion.
920 (iv) Apply the non-linear least-square method to fit the convoluted function with the out-
921 let response by adjusting the parameters iteratively. This leads to determination of
922 the RTD function, Pe and τ_h for a good agreement between the actual and the convo-
923 luted function.[110]

924 Further, the mean residence time can be obtained from the hydraulic time in the open-open sys-
925 tem[90] as

$$\tau = \tau_h \cdot \left(1 + \frac{2}{Pe}\right) \quad , \tag{54}$$

926 while the other definition of τ is given by Eq. D3 in the Appendix D. The residence times obtained
927 from Eq. 54 and D3 are consistent, which proves the validity of the RTD function as well as of
928 this algorithm. The rationality of this algorithm can be further justified by the consistency of the
929 RTD variances according to[90]

$$\sigma^2 = \tau_h^2 \cdot \left(\frac{2}{Pe} + \frac{8}{Pe^2}\right) \quad \text{, and} \tag{55}$$

$$\sigma^2 = \int_0^\infty (t-\tau)^2 \cdot f(t)dt \quad . \tag{56}$$

930 The estimation of the RTD enables computing the relative active and stagnant volumes on the
931 tray. Duduković and Felder[111] suggested the tail of the impulse response function, accountable
932 for the stagnant volume, to be truncated to acquire the active volume. Such truncation is re-
933 searcher's perception dependent, and can lead to inconsistent fractions. Sahai and Emi[112] pro-
934 posed that any fluid staying in a system for a period longer than twice the mean residence time

935 can be considered as the stagnant or dead volume. Using this theory, the relative stagnant area
936 due to the assumption of uniform froth height can be determined as

$$\phi_d = 1 - \frac{1}{\tau}\left\{\left(\int_{t=0}^{t=2\tau} f(t)dt\right)\left(\int_{t=0}^{t=2\tau} t \cdot f(t)dt\right)\right\} \quad . \tag{57}$$

937 With reference to Schubert et al.[18], two different liquid loads, i.e. 2 m^3/h and 3 m^3/h, during the
938 standard weir operation on a sieve tray at 0.72 $Pa^{1/2}$ F-factor are considered here. The applica-
939 tion of the reported approaches in this section on the experimental data yields the RTD and the
940 associated parameters as presented in Fig. 24. A good agreement between the convoluted func-
941 tion and the WMS outlet response (shown for the lower liquid flow) is apparent in Fig. 24a. On
942 comparison with higher liquid flow on the tray, lower liquid load exhibits higher residence time,
943 smaller Péclet number and larger percentage of liquid stagnancy, yet there is little difference in
944 their numerical values (refer Fig. 24b).

945

946

947

948

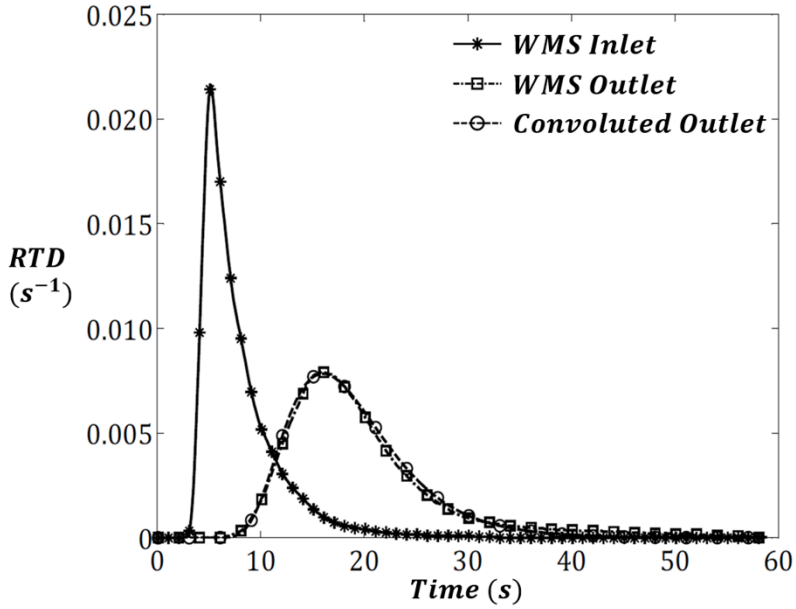

949

950 **(a)**

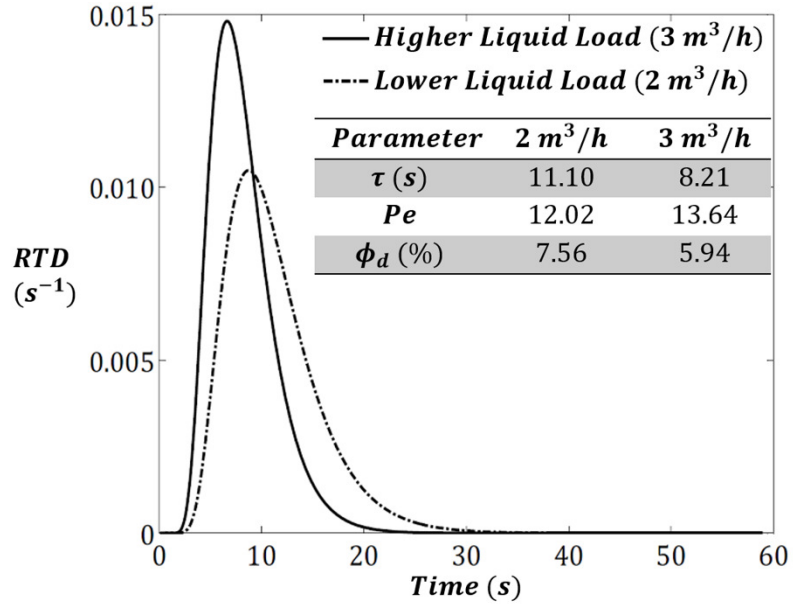

Parameter	$2\ m^3/h$	$3\ m^3/h$
$\tau\ (s)$	11.10	8.21
Pe	12.02	13.64
ϕ_d (%)	7.56	5.94

951

952 **(b)**

953 **Fig. 24.** (a) Response and convoluted function at the WMS boundaries for lower liquid flow and

954 (b) tray RTD functions with associated parameters.

955

956

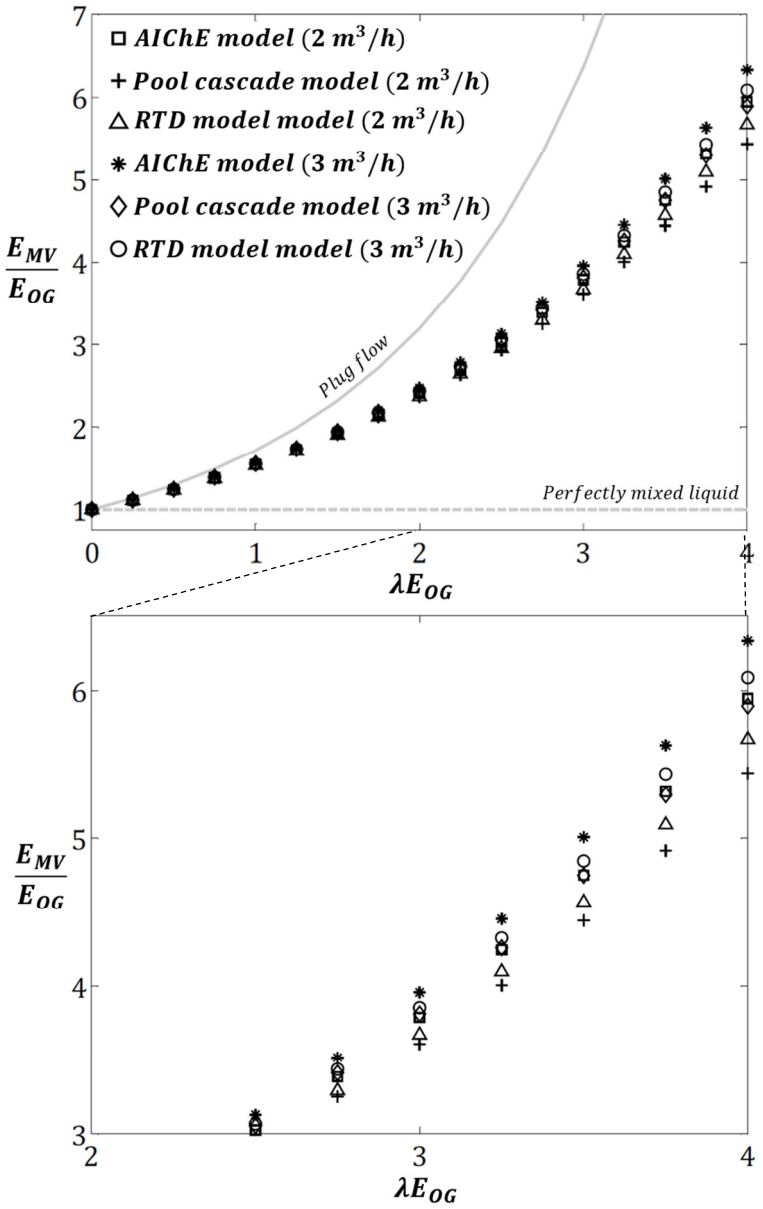

957

958
959
960 **Fig. 25.** Efficiency predictions based on the WMS data for different liquid loads

961 The RTD model, the AIChE model and the pool cascade model are used to predict the tray effi-
962 ciency for the assumed λE_{OG}. The mixed pool model is the limiting case of the pool cascade mod-
963 el for no stagnant liquid, while the eddy diffusion model requires serious computational effort
964 due to which these models are excluded from this analysis. Due to little difference in the para-
965 metric values for the considered liquid loads as in Fig. 24b, the model predictions are consistent
966 with each other for the values of λE_{OG} upto 2 as observed in Fig. 25. A slight difference in the
967 separation efficiency becomes noticeable for the λE_{OG} greater than 2, where the tray efficiency is
968 relatively higher for the higher liquid flow. This justifies that higher Péclet number and smaller

969 stagnant regions are beneficial for the tray efficiency, and vice-versa. With reference to the RTD
970 model that is considered as the most realistic and accurate model available, the AIChE model
971 and the pool cascade model slightly overpredicts and underpredicts the tray efficiency, respec-
972 tively. The overprediction of the tray efficiency by the AIChE model is upto 5%, while the effi-
973 ciency underprediction in case of the pool cascade model is upto 4% for the given range of λE_{OG}.
974 Further, the predictions from the pool model correspond to $\beta_o = 4$, which on adjustment (as in
975 Fig. 13) could predict the efficiency closer to the RTD model. Thus, an example on the extraction
976 of the fluid dynamics data from experiments and subsequent realization of the efficiency predic-
977 tions from mathematical models is hereby demonstrated.

978

979 6. Concluding Remarks and Perspective

980 Flow and mixing patterns on cross-flow trays are significant for their separation efficiency. The
981 distillation trays can no longer be perceived as black-box, as technological advances in meas-
982 urement and imaging techniques have been successful in quantifying the flow on them at high
983 spatial and temporal resolution. The experimental data needs to be processed using mathemati-
984 cal models for calculating the tray efficiency. The development of new tray efficiency models or
985 improvements in the existing ones is desired parallel to advances in CFD modeling and meas-
986 urements. In order to make these columns cost and energy efficient, an improvement in mass-
987 transfer characteristics of column trays through design modification and revamping seems to be
988 a potential nomination. This is possible after their efficiency is accounted accurately. This serves
989 as a motivation for further advancements in the efficiency modeling so that a better interpreta-
990 tion regarding the tray functioning becomes available. Further, a hybrid approach i.e. using
991 mathematical models supplemented with the fluid dynamics information from experimentally
992 validated CFD models, could be preferred in the future for tray efficiency predictions. Therefore,
993 the experimental and the simulation studies intended for column tray flow patterns have been
994 reviewed in this work. In particular, a comprehensive evaluation of the tray efficiency prediction

models has been presented by stating their formulation, strengths, weaknesses and associated analysis. Also, the dependence of the tray efficiency on system and flow properties has been discussed. Furthermore, a concise algorithm concerning the processing and utilization of the experimental data in tandem with mathematical models has been proposed. This work is anticipated to provide an insight on the tray efficiency modeling, and aims at invigorating the research in tray columns for future developments.

7. Acknowledgement

The author (V.V.) gratefully acknowledges Helmholtz-Zentrum Dresden-Rossendorf for providing the facilities to carry out this work.

Funding: This work was supported by the German Academic Exchange Service (Deutscher Akademischer Austauschdienst, DAAD) [grant number 91563198].

8. Nomenclature

A	Cross-sectional area of froth perpendicular to the flow direction (m^2)
A_b	Bubbling or perforated area of the tray (m^2)
b	Slope of the VLE line (-)
$C_{in}(t)$	Time-dependent tracer concentration at the tray (or WMS) inlet (mol/m^3)
$C_{out}(t)$	Time-dependent tracer concentration at the tray (or WMS) outlet (mol/m^3)
$c(t)$	Time-dependent tracer concentration (mol/m^3)
c_1, c_2	Constants in Appendix B (-)
D	Tray diameter (m)
D_E	Eddy diffusion coefficient (m^2/s)
E_{ML}	Liquid-side Murphree tray efficiency (-)

E_{MV}	Vapor or gas-side Murphree tray efficiency (-)
E_o	Overall column efficiency (-)
E_{OG}	Vapor or gas-side point efficiency (-)
$f(t)$	Residence time function (s^{-1})
G	Gas flow rate (kmol/s)
G'	Gas flow rate per tray bubbling area (kmol/(m^2·s))
h_F	Froth height (m)
k	Number of channels in Stichlmair's model (-)
K	Diffusion coefficient based on the size of the fluid element in the RTD model (kmol/(m^3·s))
L	Liquid flow rate (kmol/s)
L'	Liquid flow rate per unit weir length (kmol/(m·s))
m	Tray number (-)
N_{ac}	Actual number of trays in the column (-)
N_{eq}	Number of equilibrium stages in the column (-)
n	Number of pools in the flow direction (-)
$\dot{n}$	Dimensionless distance normal to the column wall (-)
Pe	Péclet number (= $Z_1^2/(D_E \cdot \tau)$ (-)
$\dot{Pe}$	Péclet number denoting the three-dimensional eddy mixing (-)
p	Arbitrary point on the tray (-)
Q	Volumetric flow rate of liquid (m^3/s)
Q_L	Volumetric flow rate of liquid per tray width (m^2/s)
q_s	Normalized slip velocity at the wall (-)
$q(\xi)$	Normalized velocity profile function (-)
$R(t)$	Response function (s^{-1})
r_1, r_2	Roots of the differential equation in Appendix B (-)
s	Non-dimensional distance in the flow direction from the inlet weir (-)

1047	T	Parameter used in Appendix A (-)
1048	t	Time (s)
1049	U	Parameter used in Appendix A (-)
1050	V_f	Average froth velocity (m/s)
1051	V_G	Gas velocity (m/s)
1052	W	Weir length (m)
1053	w	Distance from the tray centerline perpendicular to the flow direction (m)
1054	w'	Normalized distance from the tray centerline perpendicular to the flow direction
1055		$(= z/D)$ (-)
1056	X	Parameter used in Appendix B (-)
1057	x	Composition (mole fraction) of the volatile component in the liquid phase (-)
1058	x'	Composition (mole fraction) of the volatile component in the liquid phase in the
1059		side mixers (-)
1060	x_e^*	Liquid composition in equilibrium with the incoming vapor (-)
1061	x_m	Composition of liquid leaving the tray (-)
1062	x_{+m}	Liquid composition at the inlet weir (-)
1063	x_{m1}	Liquid composition at the inlet of the retrograde flow zone (-)
1064	x_{m2}	Mixing cup average composition of liquid leaving the retrograde flow zone (-)
1065	x_m^*	Liquid composition in equilibrium with vapor leaving the tray (-)
1066	x_{m-1}	Composition of liquid entering the tray (-)
1067	$\bar{x}(z)$	Space mean composition of liquid at point z (-)
1068	y	Composition (mole fraction) of the volatile component in the vapor phase (-)
1069	y'	Composition (mole fraction) of the volatile component in the vapor phase in the
1070		side mixers (-)
1071	y_m	Composition of vapor leaving the tray (-)
1072	y_m^*	Composition of vapor in equilibrium with liquid leaving the tray (-)
1073	y_{in}	Composition of vapor entering the tray (-)

y_p	Composition of vapor at point p on the tray (-)
y_p^*	Composition of vapor in equilibrium with liquid at point p on the tray (-)
y_2	Composition of vapor leaving the froth element in the AIChE model (-)
Z_1	Flow path length (m)
z	Distance from inlet weir in the flow direction (m)
z'	Normalized distance from inlet weir in the flow direction ($= z/D$) (-)

Subscripts

a	Active region on the tray
d	Stagnant region on the tray
f	Froth
h	Hydraulic
i	Channel index in the multi-channel plug flow model, index for main line mixers in the pool cascade model
in	Inlet
j	Index for pools and side mixers in the mixed stages model and the pool cascade model respectively
m	m^{th} tray
$mean$	Mean or average
w	w - direction
z	z – direction

Superscript

$*$	Equilibrium

Greek Letters

β	Fraction of liquid that circulates between main line mixer and side mixer (-)
β_o	Empirical fitting parameter in the pool cascade model (-)
γ	Parameter used in the plug flow model (-)
δ	Central tray area with forward flow per total tray area (-)
η	Parameter used in the AIChE model (-)
θ	Non-dimensional time ($= t/\tau$) (-)
λ	Stripping factor (-)
ξ	Non-dimensional distance from the tray centerline orthogonal to the flow direction (-)
ρ_L	Clear liquid density (kmol/m^3)
ρ_F	Froth density (= volume of liquid/froth volume) (-)
σ^2	Variance of the RTD function (s^2)
τ	Mean residence time of the liquid on the tray (s)
τ_h	Hydraulic or space time (= volume of the system/volumetric flow rate) (s)
ϕ_a	Relative volume of the active region in the pool cascade model (-)
ϕ_d	Relative volume of the stagnant region in the pool cascade model (-)
ψ	Stream function (m^2/s)
ψ_o	Stream function value at the column wall (m^2/s)
ω	Fraction of the recycled liquid as retrograde flow (-)

Abbreviations

$AIChE$	American Institute of Chemical Engineers
CFD	Computational fluid dynamics
LES	Large eddy simulation

MDF	Maldistribution factor
RTD	Residence time distribution
SA	Stagnant area
VLE	Vapor-liquid equilibrium
VOF	Volume of fluid
WMS	Wire mesh sensor
$2D$	Two-dimensional
$3D$	Three-dimensional

Appendix (A)

For plug flow of the liquid, the pool model transforms to

$$E_{MV} = \left[\left(1 + \frac{\phi_a \lambda E_{OG}}{n}\right)^n - 1\right]/\lambda \quad . \tag{21}$$

Taking $\phi_a \lambda E_{OG} = T$ and $U = n/T$ (used later) for simplicity, the above equation becomes

$$E_{MV} = \left[\left(1 + \frac{T}{n}\right)^n - 1\right]/\lambda \quad . \tag{A1}$$

For infinite number of pools, $\lim_{n\to\infty}\left(1+\frac{T}{n}\right)^n$ needs to be calculated as

$$\lim_{n\to\infty}\left(1+\frac{T}{n}\right)^n = \lim_{n\to\infty}\left\{\left(1+\frac{1}{n/T}\right)^{n/T}\right\}^T = \lim_{U\to\infty}\left\{\left(1+\frac{1}{U}\right)^U\right\}^T \quad . \tag{A2}$$

Using the binomial expansion, one can write

$$\left(1+\frac{1}{U}\right)^U = {}^UC_0 \cdot 1^U \cdot (1/U)^0 + {}^UC_1 \cdot 1^{U-1} \cdot (1/U)^1 + {}^UC_2 \cdot 1^{U-2} \cdot (1/U)^2 + \cdots$$

$$= 1 + 1 + \frac{U-1}{2U} + \frac{(U-1)(U-2)}{6U^2} + \cdots = 1 + 1 + \frac{1}{2} - \frac{1}{2U} + \frac{(1-1/U)(1-2/U)}{6} + \quad \ldots \tag{A3}$$

1137 The application of the limit in Eq. A3 provides

$$\lim_{U\to\infty}\left(1+\frac{1}{U}\right)^{U} = 1+1+\frac{1}{2}+\frac{1}{6}+\cdots = e^{1} \quad \text{(Maclaurin's series expansion of the exponential function).} \tag{A4}$$

1138 Using Eqs. A1 to A4, it is possible to write Eq. 21 as

$$E_{MV} = \frac{exp(\phi_a \lambda E_{OG}) - 1}{\lambda} \quad . \tag{22}$$

1139

1140 Appendix (B)

1141 The mass balance over the froth element in the AIChE model generates

$$\frac{1}{Pe}\frac{d^2x}{ds^2} - \frac{dx}{ds} - \lambda E_{OG}(x - x_e^*) = 0 \quad . \tag{27}$$

1142 By assuming $X = x - x_e^*$, Eq. 27 becomes

$$X'' - Pe\, X' - \lambda E_{OG} Pe X = 0 \quad . \tag{B1}$$

1143 The solution of Eq. B1 is given by

$$r^2 - Pe.r - Pe.\lambda E_{OG} = 0 \quad , \tag{B2}$$

$$r_1, r_2 = \frac{Pe \pm \sqrt{Pe^2 + 4Pe\ \lambda E_{OG}}}{2} \quad \text{, and} \tag{B3}$$

$$X = c_1 e^{r_1 s} + c_2 e^{r_2 s} \quad . \tag{B4}$$

1144 Here c_1 and c_2 are the constants while r_1 and r_2 are the roots of the differential equation. The

1145 application of the boundary conditions (Eqs. 28 and 29) to Eq. B4 gives

Boundary condition 1: $X(1) = x_m - x_e^* = c_1 e^{r_1} + c_2 e^{r_2}$ and (B5)

Boundary condition 2: $X'(1) = c_1 r_1 e^{r_1} + c_2 r_2 e^{r_2} = 0$. (B6)

1146 Solving the last three equations for c_1 and c_2, Eq. B7 is obtained as

$$\frac{x - x_e^*}{x_m - x_e^*} = \frac{exp\{(\eta + Pe)(s-1)\}}{1 + \frac{\eta + Pe}{\eta}} + \frac{exp\{\eta(1-s)\}}{1 + \frac{\eta}{\eta + Pe}} \quad \text{(B7)}$$

$$\text{where} \quad \eta = \frac{Pe}{2}\left(\sqrt{1 + \frac{4\lambda E_{OG}}{Pe}} - 1\right) \quad . \quad (31)$$

1147 Earlier, it has been stated that

$$y_2 - y_{in} = m(x - x_e^*)E_{OG} \quad . \quad \text{(B8)}$$

1148 Applying Eq. B8 and considering a constant vapor load of uniform composition at the tray inlet
1149 permits to formulate the tray efficiency as

$$y_m - y_{in} = \int_0^1 (y_2 - y_{in})ds = mE_{OG}\int_0^1 (x - x_e^*)ds \quad , \quad \text{(B9)}$$

$$E_{MV} = \frac{y_m - y_{in}}{y_m^* - y_{in}} = \frac{mE_{OG}\int_0^1 (x - x_e^*)ds}{m\int_0^1 (x_m - x_e^*)ds} \quad \text{, and} \quad \text{(B10)}$$

$$\frac{E_{MV}}{E_{OG}} = \frac{\int_0^1 (x - x_e^*)ds}{\int_0^1 (x_m - x_e^*)ds} \quad . \quad \text{(B11)}$$

1150 The integration on Eq. B11 using Eq. B7 result in

$$\frac{E_{MV}}{E_{OG}} = \frac{1 - exp\{-(\eta + Pe)\}}{(\eta + Pe)\left(1 + \frac{\eta + Pe}{\eta}\right)} + \frac{exp(\eta) - 1}{\eta\left(1 + \frac{\eta}{\eta + Pe}\right)} \quad . \quad (30)$$

1151

Appendix (C)

The mass balance over the froth element in the eddy diffusion model provides

$$D_E h_f \rho_L \rho_f \left(\frac{\partial^2 x}{\partial z^2} + \frac{\partial^2 x}{\partial w^2}\right) - L'_z \frac{\partial x}{\partial z} - L'_w \frac{\partial x}{\partial w} - x\left(\frac{\partial L'_z}{\partial z} + \frac{\partial L'_w}{\partial w}\right) - G'\{y(z,w) - y_{in}\} = 0 \quad . \qquad (32)$$

The equation of continuity is

$$\frac{\partial L'_z}{\partial z} + \frac{\partial L'_w}{\partial w} = 0 \quad . \qquad (C1)$$

The application of Eq. C1 transforms Eq. 32 as

$$D_E h_f \rho_L \rho_f \left(\frac{\partial^2 x}{\partial z^2} + \frac{\partial^2 x}{\partial w^2}\right) - L'_z \frac{\partial x}{\partial z} - L'_w \frac{\partial x}{\partial w} - G'(y(z,w) - y_{in}) = 0 \quad . \qquad (C2)$$

The liquid flow rates that are normal to the directions z and w, i.e. L'_z and L'_w, respectively, are replaced by stream function. This function represents a constant liquid flow with respect to the tray centerline. The equations defined for this purpose are

$$L'_z = h_f \rho_L \rho_f \frac{\partial \psi}{\partial w} \quad , \qquad (C3)$$

$$L'_w = -h_f \rho_L \rho_f \frac{\partial \psi}{\partial z} \quad , \text{and} \qquad (C4)$$

$$L = 2 h_f \rho_L \rho_f \psi_o \quad , \qquad (C5)$$

where ψ is the stream function that is measured from the centerline of the tray (it is zero at the centerline) and ψ_o is the stream function at the column wall (arbitrarily chosen).

The definitions used for E_{OG} and Pe in this model are

$$E_{OG} = \frac{y(z,w) - y_{in}}{y^* - y_{in}} = \frac{y(z,w) - y_{in}}{m(x - x_e^*)} \quad , \text{and} \qquad (C6)$$

$$Pe = \frac{DL}{h_f \rho_L \rho_f W D_E} \quad . \tag{C7}$$

Further, the directional variables are normalized by the tray diameter as

$$z' = \frac{z}{D} \quad \text{, and} \tag{C8}$$

$$w' = \frac{w}{D} \quad . \tag{C9}$$

The application of Eqs. C3 to C9 in Eq. C2 produces Eq. 33 as

$$\frac{1}{Pe}\left(\frac{\partial^2 x}{\partial z'^2} + \frac{\partial^2 x}{\partial w'^2}\right) - \frac{W}{2D\psi_o}\left(\frac{\partial \psi}{\partial w'}\frac{\partial x}{\partial z'} - \frac{\partial \psi}{\partial z'}\frac{\partial x}{\partial w'}\right) - \frac{\lambda E_{OG} W D (x - x_e^*)}{A_b} = 0 \quad . \tag{33}$$

Appendix (D)

The material balance over the elemental volume in the RTD model results in

$$Lf(t)dt\left\{\frac{\partial x(z,t)}{\partial z}dz\right\} + dG\{y(z,t) - y_{in}\}\frac{dz}{Z_1} + KdAdz\{x(z,t) - \bar{x}(z)\} = 0 \quad . \tag{46}$$

Using Eq. 45 to eliminate dA and dG, the usual definitions of point efficiency, stripping factor and linear VLE relationship, Eq. 47 and assuming $s = z/Z_1$, the above equation becomes

$$f(t)\left[\frac{dx(s,t)}{ds} + \lambda E_{OG}\frac{t}{\tau}\{x(s,t) - x_e^*\} + \frac{KAZ_1}{L}\frac{t}{\tau}\left\{x(s,t) - \int_0^\infty x(s,t)\frac{t}{\tau}f(t)dt\right\}\right]dt = 0 \quad . \tag{D1}$$

Eq. D1 is integrated over time to account for all fluid elements as

$$\int_0^\infty f(t)\left[\frac{dx(s,t)}{ds} + \lambda E_{OG}\frac{t}{\tau}\{x(s,t) - x_e^*\} + \frac{KAZ_1}{L}\frac{t}{\tau}\left\{x(s,t) - \int_0^\infty x(s,t)\frac{t}{\tau}f(t)dt\right\}\right]dt = 0 \quad . \tag{D2}$$

The mean residence time is defined as

$$\tau = \int_0^\infty t f(t) dt \quad . \tag{D3}$$

Using Eq. D3, Eq. D2 transforms to

$$\int_0^\infty f(t) \left[\frac{dx(s,t)}{ds} + \lambda E_{OG} \frac{t}{\tau} \{ x(s,t) - x_e^* \} \right] dt = 0 \quad . \tag{D4}$$

Since $0 < t < \infty$ and $f(t) \geq 0$, it is appropriate to write the above equation as

$$\frac{dx(s,t)}{ds} + \lambda E_{OG} \frac{t}{\tau} \{ x(s,t) - x_e^* \} = 0 \quad . \tag{D5}$$

Eq. D5 can be solved by the method of separation of variables. Its solution and boundary condition at the inlet are straightforward and can be easily understood from Eq. D6 as

$$\frac{x(s\,,t) - x_e^*}{x_{m-1} - x_e^*} = exp(-\lambda E_{OG} s\, t/\tau) \quad . \tag{D6}$$

The Murphree efficiency for the liquid-side is

$$E_{ML} = \frac{x_m - x_{m-1}}{x_m^* - x_{m-1}} \quad . \tag{D7}$$

The average composition of liquid exiting the tray can be found using Eq. D6 as

$$x_m = \int_0^\infty x(1,t) f(t) dt = \; x_e^* + (x_{m-1} - x_e^*) \int_0^\infty exp(-\lambda E_{OG}\, t/\tau)\, f(t) dt \quad . \tag{D8}$$

The only information required to relate Eq. D8 and Eq. D7 is x_m^*, which can be acquired by following the material balance over the whole tray (refer Fig. D1) as

$$L(x_m - x_{m-1}) = G(y_{in} - y_m) = mG(x_e^* - x_m^*) \quad . \tag{D9}$$

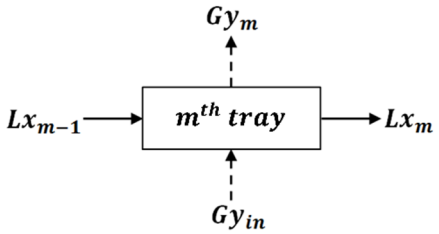

Fig. D1. Material balance over the tray boundaries.

The final expression for the tray efficiency is derived using Eqs. D7 to D9 as

$$E_{ML} = \frac{1 - \int_0^\infty \exp(-\lambda E_{OG}\, t/\tau)\,.\,f(t)dt}{1 - \frac{1}{\lambda}\left\{1 - \int_0^\infty \exp(-\lambda E_{OG}\, t/\tau)\,.\,f(t)dt\right\}} \quad . \tag{D10}$$

Following a similar procedure, the vapor-side tray efficiency can be arranged as

$$E_{MV} = \frac{1 - \int_0^\infty \exp(-\lambda E_{OG}\, t/\tau)\,.\,f(t)dt}{\lambda \int_0^\infty \exp(-\lambda E_{OG}\, t/\tau)\,.\,f(t)dt} \quad . \tag{D11}$$

References

1. Olujić Ž, Kaibel B, Jansen H, Rietfort T, Zich E, Frey G. Distillation column internals/configurations for process intensification. *Chemical Biochemical Engineering Quarterly.* 2003;17(4):301-309.
2. Górak A, Sorensen E. *Distillation: fundamentals and principles.* Academic Press; 2014.
3. Kister HZ. *Distillation design.* McGraw-Hill New York; 1992.
4. Masoumi ME, Kadkhodaie S. Optimization of energy consumption in sequential distillation column. *World Academy of Science, Engineering and Technology, International Journal of Chemical, Molecular, Nuclear, Materials and Metallurgical Engineering.* 2012;6(1):55-59.
5. Lockett MJ. *Distillation tray fundamentals.* Cambridge University Press; 1986.
6. Murphree E. Rectifying column calculations. *Industrial and Engineering Chemistry.* 1925;17(7):747-750.

7. Brambilla A. The effect of vapour mixing on efficiency of large diameter distillation plates. *Chemical Engineering Science.* 1976;31(7):517-523.

8. Onda K, Sada E, Takahashi K, Mukhtar SA. Plate and column efficiencies of continuous rectifying columns for binary mixtures. *AIChE Journal.* 1971;17(5):1141-1152.

9. Fisher KS, Rochelle GT. Effect of mixing on efficiencies for reactive tray contactors. *AIChE Journal.* 2002;48(11):2537-2544.

10. Stichlmair J, Ulbrich S. Liquid channelling on trays and its effect on plate efficiency. *Chemical Engineering and Technology.* 1987;10(1):33-37.

11. Hausen H. Zur definition des austauschgrades von rektifizierböden bei zwei-und dreistoff-gemischen. *Chemie Ingenieur Technik.* 1953;25(10):595-597.

12. Standart G. Generalized definition of a theoretical plate or stage of contacting equipment. *Chemical Engineering Science.* 1965;20(6):611-622.

13. Holland CD, McMahon KS. Comparison of vaporization efficiencies with Murphree-type efficiencies in distillation—I. *Chemical Engineering Science.* 1970;25(3):431-436.

14. Holland CD. *Fundamentals of multicomponent distillation.* McGraw-Hill; 1981.

15. Jaćimović BM, Genić SB. Normalized efficiency for stagewise operations. *Industrial and Engineering Chemistry Research.* 2011;50(12):7437-7444.

16. Jaćimović BM, Genić SB. Tray efficiency versus stripping factor. *Industrial and Engineering Chemistry Research.* 2011;50(12):7445-7451.

17. Nandakumar K, Chuang KT. Tray columns: performance. *Hydrocarbon Processing.* 2000;65(43):1140-1145.

18. Schubert M, Piechotta M, Beyer M, Schleicher E, Hampel U, Paschold J. An imaging technique for characterization of fluid flow pattern on industrial-scale column sieve trays. *Chemical Engineering Research and Design.* 2016;111:138-146.

19. Müller EA, Cavero A, Antonio Estévez L. Improving flow patterns in a distillation tray by modifying downcomer apron shape. *Chemical Engineering Communications.* 1988;74(1):195-208.

20. Lockett MJ, Safekourdi A. The effect of the liquid flow pattern on distillation plate efficiency. *Chemical Engineering Journal.* 1976;11(2):111-121.

21. Porter KE, Lockett MJ, Lim CT. The effect of liquid channeling on distillation plate efficiency. *Transactions of the Institution of Chemical Engineers.* 1972;50(2):91-101.

22. Sohlo J, Kinnunen S. Dispersion and flow phenomena on a sieve plate. *Transactions of the Institution of Chemical Engineers.* 1977;55:71-73.

23. Porter KE, Yu KT, Chambers S, Zhang MQ. Flow patterns and temperature profiles on a 2.44 m diameter sieve tray. *Chemical Engineering Research and Design.* 1992;70(A):489-500.

24. Li Y, Wang L, Yao K. New technique for measuring fluid flow patterns on a multiple downcomer tray. *Industrial and Engineering Chemistry Research.* 2007;46(9):2892-2897.

25. Biddulph MW, Bultitude DP. Flow characteristics of a small-hole sieve tray. *AIChE Journal.* 1990;36(12):1913-1916.

26. Solari RB, Bell RL. Fluid flow patterns and velocity distribution on commercial-scale sieve trays. *AIChE Journal.* 1986;32(4):640-649.

27. Bell RL. Experimental determination of residence time distributions on commercial scale distillation trays using a fiber optic technique. *AIChE Journal.* 1972;18(3):491-497.

28. Bell RL. Residence time and fluid mixing on commercial scale sieve trays. *AIChE Journal.* 1972;18(3):498-505.

29. Yu KT, Huang J, Li JL, Song HH. Two-dimensional flow and eddy diffusion on a sieve tray. *Chemical Engineering Science.* 1990;45(9):2901-2906.

30. Liu C, Yuan X, Yu KT, Zhu X. A fluid–dynamic model for flow pattern on a distillation tray. *Chemical Engineering Science.* 2000;55(12):2287-2294.

31. Mehta B, Chuang K, Nandakumar K. Model for liquid phase flow on sieve trays. *Chemical Engineering Research and Design.* 1998;76(7):843-848.

32. Krishna R, Van Baten J, Ellenberger J, Higler A, Taylor R. CFD simulations of sieve tray hydrodynamics. *Chemical Engineering Research and Design.* 1999;77(7):639-646.

33. Van Baten J, Krishna R. Modelling sieve tray hydraulics using computational fluid dynamics. *Chemical Engineering Journal.* 2000;77(3):143-151.

34. Gesit G, Nandakumar K, Chuang KT. CFD modeling of flow patterns and hydraulics of commercial-scale sieve trays. *AIChE Journal.* 2003;49(4):910-924.

35. Wang XL, Liu CJ, Yuan XG, Yu K. Computational fluid dynamics simulation of three-dimensional liquid flow and mass transfer on distillation column trays. *Industrial and Engineering Chemistry Research.* 2004;43(10):2556-2567.

36. Rahimi R, Rahimi MR, Zivdar M. Efficiencies of sieve tray distillation columns by CFD simulation. *Chemical Engineering and Technology.* 2006;29(3):326-335.

37. Noriler D, Meier H, Barros A, Maciel MW. Thermal fluid dynamics analysis of gas–liquid flow on a distillation sieve tray. *Chemical Engineering Journal.* 2008;136(2):133-143.

38. Noriler D, Barros AA, Maciel MRW, Meier HF. Simultaneous momentum, mass, and energy transfer analysis of a distillation sieve tray using CFD techniques: prediction of efficiencies. *Industrial and Engineering Chemistry Research.* 2010;49(14):6599-6611.

39. Li X, Yang N, Sun Y, Zhang L, Li X, Jiang B. Computational fluid dynamics modeling of hydrodynamics of a new type of fixed valve tray. *Industrial and Engineering Chemistry Research.* 2013;53(1):379-389.

40. Ping Z, Dan J, Huibo M, Jianhua W. Three-dimensional simulation of liquid flow on a sieve tray under different inclinations. *Brazilian Journal of Chemical Engineering.* 2014;31(4):905-912.

41. Li Q, Li L, Zhang M, Lei Z. Modeling flow-guided sieve tray hydraulics using computational fluid dynamics. *Industrial and Engineering Chemistry Research.* 2014;53(11):4480-4488.

42. Zarei T, Abedini E, Rahimi R, Khorshidi J. Computational fluid dynamics on the hydrodynamic characteristics of the conical cap tray. *Korean Journal of Chemical Engineering.* 2017;34(4):969-976.

43. Bennett D, Agrawal R, Cook P. New pressure drop correlation for sieve tray distillation columns. *AIChE Journal.* 1983;29(3):434-442.

44. Colwell CJ. Clear liquid height and froth density on sieve trays. *Industrial and Engineering Chemistry Process Design and Development.* 1981;20(2):298-307.

45. Schultes M. Research on mass transfer columns: passé? *Chemical Engineering and Technology.* 2013;36(9):1539-1549.

46. Sakata M, Yanagi T. Performance of a commercial scale sieve tray. Paper presented at: Instituion of Chemical Engineers Symposium Series1979.

47. Taylor R. (Di) Still modeling after all these years: a view of the state of the art. *Industrial and Engineering Chemistry Research.* 2007;46(13):4349-4357.

48. Zarei T, Rahimi R, Zivdar M. Computational fluid dynamic simulation of MVG tray hydraulics. *Korean Journal of Chemical Engineering.* 2009;26(5):1213.

49. Rahimi R, Sotoodeh MM, Bahramifar E. The effect of tray geometry on the sieve tray efficiency. *Chemical Engineering Science.* 2012;76:90-98.

50. Jiang S, Gao H, Sun J, Wang Y, Zhang L. Modeling fixed triangular valve tray hydraulics using computational fluid dynamics. *Chemical Engineering and Processing: Process Intensification.* 2012;52:74-84.

51. Jiang B, Liu P, Zhang L, et al. Hydrodynamics and mass-transfer analysis of a distillation ripple tray by computational fluid dynamics simulation. *Industrial and Engineering Chemistry Research.* 2013;52(49):17618-17626.

52. Sun J, Luo X, Jiang S, et al. Computational fluid dynamics hydrodynamic analysis of a cross-orthogonal fixed-valve tray. *Chemical Engineering and Technology.* 2014;37(3):383-391.

53. Albadawi A, Donoghue D, Robinson A, Murray D, Delauré Y. Influence of surface tension implementation in volume of fluid and coupled volume of fluid with level set methods for bubble growth and detachment. *International Journal of Multiphase Flow.* 2013;53:11-28.

54. Malvin A, Chan A, Lau PL. CFD study of distillation sieve tray flow regimes using the droplet size distribution technique. *Journal of the Taiwan Institute of Chemical Engineers.* 2014;45(4):1354-1368.

55. Li X, Cong H, Gao X, Li H. Investigation and simulation on the performance of the elliptical tray placed in the unconventional "s" shape distillation column. *Journal of the Taiwan Institute of Chemical Engineers.* 2016;60:44-58.

56. Zarei T, Rahimi R, Zarei A, Zivdar M. Hydrodynamic characteristic of Conical Cap tray: Experimental studies on dry and total pressure drop, weeping and entrainment. *Chemical Engineering and Processing: Process Intensification.* 2013;64:17-23.

57. Lockett MM, Dhulesia HA. Murphree Plate Efficiency with Nonuniform Vapour Distribution. *Chemical Engineering Journal.* 1980;19(3):183-188.

58. Safekourdi A. *The effect of liquid flow pattern on distillation plate efficiency* [Doctoral dissertation], The Victoria University of Manchester; 1975.

59. Kirschbaum E. Efficiency of Rectification and Appropriate Path for Liquid Flow. *Forschung auf dem Gebiete des Ingenieurwesens.* 1934;5:245.

60. Lewis Jr WK. Rectification of binary mixtures. *Industrial and Engineering Chemistry.* 1936;28(4):399-402.

61. King CJ. *Separation processes.* Courier Corporation; 2013.

62. Olujic Z, Van Baak R, Haaring J. Liquid distribution behaviour of conventional and high capacity structured packings. *Institution of Chemical Engineers.* 2006;152:252-266.

63. Kirschbaum E. *Distillation and rectification.* Chemical Publishing Company; 1948.

64. Gautreaux MF, O'Connell HE. Effect of length of liquid path on plate efficiency. *Chemical Engineering Progress.* 1955;51(5):232-237.

65. Gunness R. Column performance in the rectification of petroleum. *Industrial and Engineering Chemistry.* 1937;29(10):1092-1100.

66. Miyauchi T, Vermeulen T. Longitudinal dispersion in two-phase continuous-flow operations. *Industrial and Engineering Chemistry Fundamentals.* 1963;2(2):113-126.

67. Bruin S, Freije AD. A simple liquid mixing model for distillation plates with stagnant zones. *Transactions of the Institution of Chemical Engineers.* 1974;52:75-79.

68. Ashley MJ, Haselden GG. The calculation of plate efficiency under conditions of finite mixing in both phases in multiplate columns, and the potential advantage of parallel flow. *Chemical Engineering Science.* 1970;25(11):1665-1672.

69. AIChE. *Bubble-tray Design Manual - Prediction of fractionation efficiency.* American Institute of Chemical Engineers; 1958.

70. Molnar K. Eddy-diffusion coefficient in valve tray distillation columns. *Periodica Polytechnica Mechanical Engineering.* 1974;18(2-3):155-166.

71. Barker PE, Self MF. The evaluation of liquid mixing effects on a sieve plate using unsteady and steady state tracer techniques. *Chemical Engineering Science.* 1962;17(7):541-554.

72. Bennett DL, Grimm HJ. Eddy diffusivity for distillation sieve trays. *AIChE Journal.* 1991;37(4):589-596.

73. Foss AS, Gerster JA, Pigford RL. Effect of liquid mixing on the performance of bubble trays. *AIChE Journal.* 1958;4(2):231-239.

74. Gerster JA, Hill AB, Hochgraf NN, Robinson DG. *Tray Efficiencies in Distillation Columns-Final Report from the University of Delaware.* American Institute of Chemical Engineers;1958.

75. Gilbert T. Liquid mixing on bubble-cap and sieve plates. *Chemical Engineering Science.* 1959;10(4):243-253.

76. Welch N, Durbin L, Holland C. Mixing on valve trays and in downcomers of a distillation column. *AIChE Journal.* 1964;10(3):373-379.

77. Harada M, Adachi M, Eguchi W, Nagata S. Studies of fluid mixing on sieve plates. *International Chemical Engineering.* 1964;4(1):165.

78. Sterbacek Z. Liquid dispersion coefficients on perforated plates with downcomers. *Transactions of the Institution of Chemical Engineers.* 1968;46(5):T167.

79. Zuiderweg F. Sieve trays: a view on the state of the art. *Chemical Engineering Science.* 1982;37(10):1441-1464.

80. Zuiderweg F, de Groot J, Meeboer B, van der Meer D. Scaling up distillation plates. Paper presented at: Proceedings of the International Symposium on Distillation, England1969.

81. Wehner JF, Wilhelm RH. Boundary conditions of flow reactor. *Chemical Engineering Science.* 1956;6(2):89-93.

82. Lim CT, Porter KE, Lockett MJ. The effect of liquid channelling on two-pass distillation plate efficiency. *Transactions of the Institution of Chemical Engineers.* 1974;52:193-201.

83. Solari RB. *Liquid mixing and efficiency on non-ideal distillation trays* [Doctoral dissertation], University of California, Davis; 1974.

84. Bell RL, Solari RB. Effect of nonuniform velocity fields and retrograde flow on distillation tray efficiency. *AIChE Journal.* 1974;20(4):688-695.

85. Foss AS. *Liquid mixing on bubble trays and its effect upon plate efficiency* [Doctoral dissertation], University of Delaware; 1957.

86. Stewart GN. Researches on the circulation time in organs and on the influences which affect it: Parts I—III. *The Journal of Physiology.* 1893;15(1-2):1.

87. MacMullin RB, Weber M. The theory of short-circuiting in continuous-flow mixing vessels in series and the kinetics of chemical reactions in such systems. *Transactions of the American Institute of Chemical Engineers.* 1935;31(2):409-458.

88. Andersen SL, Matthias RH. Prediction of catalyst activity in fluidized systems employing constant catalyst replacement rate. *Industrial and Engineering Chemistry.* 1954;46(6):1296-1298.

89. Danckwerts PV. Continuous flow systems: distribution of residence times. *Chemical Engineering Science.* 1953;2(1):1-13.

90. Levenspiel O. *Chemical reaction engineering.* 3rd ed: John Wiley and Sons; 1999.

91. Fogler HS, Gürmen MN. *Elements of chemical reaction engineering (online version).* 4th ed: University of Michigan; 2008.

92. Foss A, Gerster J. Liquid film efficiencies on sieve trays. *Chemical Engineering Progress.* 1956;52(1):28.

93. Paul EL, Atiemo-Obeng VA, Kresta SM. *Handbook of industrial mixing: science and practice.* John Wiley and Sons; 2004.

94. Azizi F, Abou Hweij K. Liquid-phase axial dispersion of turbulent gas–liquid co-current flow through screen-type static mixers. *AIChE Journal.* 2017;63(4):1390-1403.

95. Thakur R, Vial C, Nigam K, Nauman E, Djelveh G. Static mixers in the process industries—a review. *Chemical Engineering Research and Design.* 2003;81(7):787-826.

96. Häfeli R, Hutter C, Damsohn M, Prasser H-M, von Rohr PR. Dispersion in fully developed flow through regular porous structures: experiments with wire-mesh sensors. *Chemical Engineering and Processing: Process Intensification.* 2013;69:104-111.

97. Bennia A, Nahman N. Deconvolution of system impulse responses and time domain waveforms. *IEEE Transactions on Instrumentation and Measurement.* 1990;79:933-939.

98. Bošković D, Loebbecke S. Modelling of the residence time distribution in micromixers. *Chemical Engineering Journal.* 2008;135:S138-S146.

99. Essadki AH, Gourich B, Vial C, Delmas H. Residence time distribution measurements in an external-loop airlift reactor: Study of the hydrodynamics of the liquid circulation induced by the hydrogen bubbles. *Chemical Engineering Science.* 2011;66(14):3125-3132.

100. Heibel AK, Lebens PJ, Middelhoff JW, Kapteijn F, Moulijn J. Liquid residence time distribution in the film flow monolith reactor. *AIChE journal.* 2005;51(1):122-133.

101. Hutter C, Zenklusen A, Lang R, von Rohr PR. Axial dispersion in metal foams and streamwise-periodic porous media. *Chemical Engineering Science.* 2011;66(6):1132-1141.

102. Mills P, Duduković M. Convolution and deconvolution of nonideal tracer response data with application to three-phase packed-beds. *Computers and Chemical Engineering.* 1989;13(8):881-898.

103. Mao Z-S, Xiong T, Chen J. Residence time distribution of liquid flow in a trickle bed evaluated using FFT deconvolution. *Chemical Engineering Communications.* 1998;169(1):223-244.

104. Parruck B, Riad SM. Study and performance evaluation of two iterative frequency-domain deconvolution techniques. *IEEE Transactions on Instrumentation and Measurement.* 1984;33(4):281-287.

105. Pananakis D, Abel E. A comparison of methods for the deconvolution of isothermal DSC data. *Thermochimica Acta.* 1998;315(2):107-119.

106. Saber M, Pham-Huu C, Edouard D. Axial dispersion based on the residence time distribution curves in a millireactor filled with β-SiC foam catalyst. *Industrial and Engineering Chemistry Research.* 2012;51(46):15011-15017.

107. Gutierrez CG, Dias EF, Gut JA. Residence time distribution in holding tubes using generalized convection model and numerical convolution for non-ideal tracer detection. *Journal of Food Engineering.* 2010;98(2):248-256.

108. Georget E, Sauvageat JL, Burbidge A, Mathys A. Residence time distributions in a modular micro reaction system. *Journal of Food Engineering.* 2013;116(4):910-919.

109. Levenspiel O, Smith W. Notes on the diffusion-type model for the longitudinal mixing of fluids in flow. *Chemical Engineering Science.* 1957;6(4-5):227-235.

110. Mohammed I, Bauer T, Schubert M, Lange R. Hydrodynamic multiplicity in a tubular reactor with solid foam packings. *Chemical Engineering Journal.* 2013;231:334-344.

111. Dudukovic M, Felder R. Mixing effects in chemical reactors - IV - residence time distributions. *Reactor Stability, Sensitivity and Mixing Effects*: AIChE Modular Instruction Series; 1983:50-61.

112. Sahai Y, Emi T. Melt flow characterization in continuous casting tundishes. *ISIJ international.* 1996;36(6):667-672.